

Supporting Information for:

**Simultaneously controlling conformational and operational stability
of single-chain polymeric nanoparticles in complex media**

Stefan Wijker,^a Rico Monnink,^a Luc Rijnders,^a Linlin Deng,^a and Anja R.A. Palmans^{*a}

a. Institute for Complex Molecular Systems, Laboratory of Macromolecular and Organic Chemistry, Eindhoven University of Technology, P.O. Box 513, 5600 MB, Eindhoven, The Netherlands.

*To whom correspondence should be addressed

E-mail: a.palmans@tue.nl

Table of Contents

1. Materials and methods	3
1.1. Materials	3
1.2. Methods	3
2. Experimental Section	5
2.1. Synthesis of small molecules and monomers	5
2.2. Synthesis of random heterograft copolymers	15
2.3. Nanoparticle size	20
2.4. Synthesis of pyrazoline adduct	21
2.5. Pyrazoline solvatochromism	22
2.6. Pyrazoline UV-vis absorbance spectrum, extinction coefficient, and quantum yield	23
2.7. Pyrazoline formation in P1 and P3	25
2.8. Pyrazoline adduct long-term stability	27
3. References	27

1. Materials and methods

1.1. Materials

Furan-2,5-dione (99.5%, Fischer), furan (99%, Aldrich), methyl tert-butyl ether (99%, Acros), ethanolamine (99%, Aldrich), anhydrous magnesium sulphate (99%, Acros), triethyl amine (99.5%, Aldrich), methacryloyl chloride (97%, Aldrich), 4-formylbenzoic acid (97%, Aldrich), dry dimethylformamide (99%, Biosolve), 2-bromoethanol (95%, Aldrich), sodium hydrogen carbonate (Aldrich), dry diethyl ether (99%, Biosolve), p-toluenesulfonyl hydrazide (99%, Aldrich), pyridine (99%, Biosolve), p-anisidine (99%, Aldrich), hydrogen chloride solution (5M, VWR), sodium nitrite (97%, Aldrich), dodecyl methacrylate (96%, Aldrich), poly(ethylene glycol) methyl ether methacrylate $M_n = 500$ (Aldrich), 4-cyano-4-(phenylcarbonothioylthio)pentanoic acid (97%, Aldrich), 4-cyano-4-(phenylcarbonothioylthio)pentanoic acid N-succinimidyl ester (96%, Aldrich) anhydrous 1,4-dioxane (99%, Biosolve), phosphate buffered saline tablets (Fischer), Dulbecco's Modified Eagle Medium (Thermo Fisher Scientific), Fetal Bovine Serum (Thermo Fisher Scientific) were used without further purification. Azobisisobutyronitril (98%, Merck) was recrystallized from methanol. Dry solvents were obtained from the M-Braun dry solvent system (MB SPS-800) over a silica/alumina column. Deuterated solvents were purchased from Cambridge Isotopes Laboratories. Other solvents were purchased from Biosolve.

1.2. Methods

1.2.1. Nuclear Magnetic Resonance (NMR) Spectroscopy. ^1H NMR and ^{13}C NMR spectra were recorded on a Bruker Varian 400MR 400 MHz or a Bruker Varian Mercury Vx 400 MHz (400 MHz for ^1H NMR, 100 MHz for ^{13}C NMR). ^1H NMR and ^{13}C NMR chemical shifts are reported in ppm downfield from tetramethylsilane (TMS) as internal reference. The deuterated solvent used is indicated for each spectrum. For the abbreviations used: s = singlet, d = doublet, dd = double doublet, t = triplet, q = quartet, m = multiplet.

1.2.2. Attenuated Total Reflection - Fourier Transform Infrared (FTIR) Spectroscopy. ATR-FTIR spectra were recorded in ATR mode on a PerkinElmer FT-IR Spectrum Two equipped with a PerkinElmer UATR Two (4000 – 450 cm^{-1} , 16 scans).

1.2.3. Matrix Assisted Laser Desorption/Ionization Time of Flight Mass Spectra (MALDI-TOF-MS). MALDI-TOF-MS spectra were recorded on a Bruker Autoflex Speed MALDI-TOF instrument equipped with a 355 nm Nd:YAG smartbeam laser. The laser had a maximum repetition rate of 1 kHz. α -cyano-4-hydroxycinnamic acid (CHCA) and trans-2-[3-(4-tert-butylphenyl)-2-methyl-2-propenylidene]malononitrile (DCTB) were used as sample matrices. Samples were prepared as 1 mg mL^{-1} solutions in acetonitrile.

1.2.4. Size Exclusion Chromatography (SEC). SEC measurements in DMF were carried out on a Shimadzu prominence-I LC-2030C 3D system operated at 50 °C equipped with a Shimadzu RID-10A RI detector and a LC-2030/2040 PDA detector on a Shodex SEC-KD-804 column (exclusion limit = 400 kDa, i.d. = 0.8 cm, L = 300 mm), with DMF as eluent containing 10 mM LiBr at a constant flow rate of 1 mL min^{-1} . The column was calibrated against poly(ethylene oxide) (PEO) (Polymer Laboratories).

1.2.5. UV-vis Spectroscopy. UV-vis spectra were recorded on a Jasco V-650 spectrophotometer or a Jasco V-750 spectrophotometer (200 nm min⁻¹ scanning speed, 3 accumulations), or an Agilent Cary 3500 UV-Vis spectrophotometer (3000 nm min⁻¹ scanning speed, 1 accumulation). Quartz cuvettes with a pathlength of 1 cm were used. Standard baseline corrections were performed.

1.2.6. Fluorescence Spectroscopy. Fluorescence spectra were recorded on a Varian Cary Eclipse fluorescence spectrophotometer. The excitation wavelength 440 nm (scanning speed 200 nm min⁻¹, 5 nm slit width). Quartz cuvettes with a pathlength of 1 cm x 1 cm were used.

1.2.7. Dynamic Light Scattering (DLS). Dynamic Light Scattering measurements were recorded on a Malvern Instruments Zetasizer μ V equipped with a $\lambda = 830$ nm laser in Sarstedt disposable cuvettes after sample filtration to remove dust at 20°C. The scattering intensity was recorded as a function of the scattering vector $q = 4\pi \sin(\vartheta/2)/\lambda$, with ϑ the scattering angle in degrees and λ the wavelength of the laser in nm. The scattering intensity was recorded in triplicate, at a scattering angle of 90°, at 13 measurements of 3 seconds each. The fluctuations in the scattering intensity were automatically analyzed by the built-in CUMULANT algorithm to obtain the intensity, volume, and number distributions. The apparent hydrodynamic radius R_H was calculated from the diffusion coefficient of the particles D as $R_H = k_B T / (6\pi\eta D)$, with k_B the Boltzmann constant, T the temperature of the solution in K, and η the solvent viscosity. The final R_H was taken from the intensity distribution as average of the three measurements.

1.2.8. Delivery of Nanoparticles to HeLa cells. HeLa cells were seeded in a μ -Slide 8-well (Ibidi) plate at a density of 25000 cells per well containing 200 μ L of cell culture medium (DMEM supplemented with 10% FBS). The plate was then placed at 37 °C with 5% CO₂ flow in an oven for 24 h. After 24 h, the cell culture medium was replaced with DMEM supplemented with 10% FBS containing 3 mg mL⁻¹ nanoparticles. The plate was then placed back in the oven. After 24 h, the medium was discarded and PBS was added to wash the cells before taken confocal microscopy images.

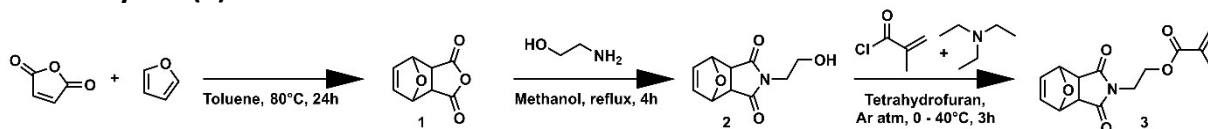
1.2.9. Confocal Microscopy Imaging. Live cell images were taken by a Leica TCS SP5 AOBS equipped with a 63 \times water immersion objective. The excitation wavelength was set at 405 nm, and emission sequence images were collected from 455 to 745 nm using the high-sensitivity HyD detector under xy λ scan mode. The sequence images were plotted in Image J to show the emission spectra.

1.2.10. Column chromatography. Automated column chromatography was performed with a Biotage Isolera One using Biotage Silica cartridges or a Buchi Grace Reveleris X2 using HP silica cartridges.

2. Experimental Section

2.1. Synthesis of small molecules and monomers

2.1.1. Synthesis of 2-(1,3-dioxo-1,3,3a,4,7,7a-hexahydro-2H-4,7-epoxyisoindol-2-yl)ethyl methacrylate (**3**)



Intermediates **1** and **2** were synthesized following literature procedures of Bolm *et al.*¹ and Mantovani *et al.*² respectively.

For compound **3**, 705 mg of **2** (3.37 mmol, 1.00 eq.) was dissolved in 10 mL dry THF under argon atmosphere in a 100 mL round-bottom flask. 0.47 mL dry TEA (3.37 mmol, 1.00 eq.) in 10 mL dry THF was added. The mixture was cooled to 0 °C in an ice bath. 0.40 mL methacryloyl chloride used as received (4.05 mmol, 1.20 eq.) was added dropwise using a dropping funnel. After addition, the mixture was stirred for 3 h at 40 °C. The reaction mixture was added to 20 mL water and extracted using 30 mL dichloromethane. The organic layer was washed three times with 10 mL water, then dried over anhydrous magnesium sulphate. The solvent was removed under reduced pressure. The product was purified by flash column chromatography (SiO₂, 1:2 heptane : ethyl acetate) to yield **3** as a viscous transparent oil (0.86 g, 92%).

2: ¹H-NMR (400 MHz, CDCl₃): δ 6.53 (s, 2H), 5.29 (s, 2H), 3.78 (t, J = 5.3 Hz, 2H), 3.75 – 3.63 (m, 2H), 2.90 (s, 2H), 2.11 (s, 1H). ¹³C-NMR (399 MHz, CDCl₃): δ 176.80, 136.54, 81.01, 60.44, 47.51, 41.82. FTIR: $\tilde{\nu}$ = 3476, 2972, 1686, 1436, 1405, 1169, 1054, 1015, 876, 807, 723, 654, 488. MALDI-TOF-MS: Found [M+Na]⁺ = 232.11 m/z. Calculated [M] = 209.07 u, [M+Na]⁺ = 232.06 u.

3: ¹H-NMR (400 MHz, CDCl₃): δ 6.51 (s, 2H), 6.07 (s, 1H), 5.59 – 5.53 (m, 1H), 5.26 (s, 2H), 4.30 (q, J = 5.9, 5.4 Hz, 2H), 3.92 – 3.68 (m, 2H), 2.86 (s, 2H), 1.90 (d, J = 1.4 Hz, 2H). ¹³C-NMR (399 MHz, CDCl₃): δ 175.93, 166.99, 136.55, 135.86, 126.06, 80.91, 60.89, 47.45, 37.79, 18.18. FTIR: $\tilde{\nu}$ = 2986, 1777, 1698, 1637, 1428, 1398, 1153, 1021, 877, 733, 649, 596. MALDI-TOF-MS: Found [M+Na]⁺ = 300.09 m/z. Calculated [M] = 277.10 u, [M+Na]⁺ = 300.09 u.

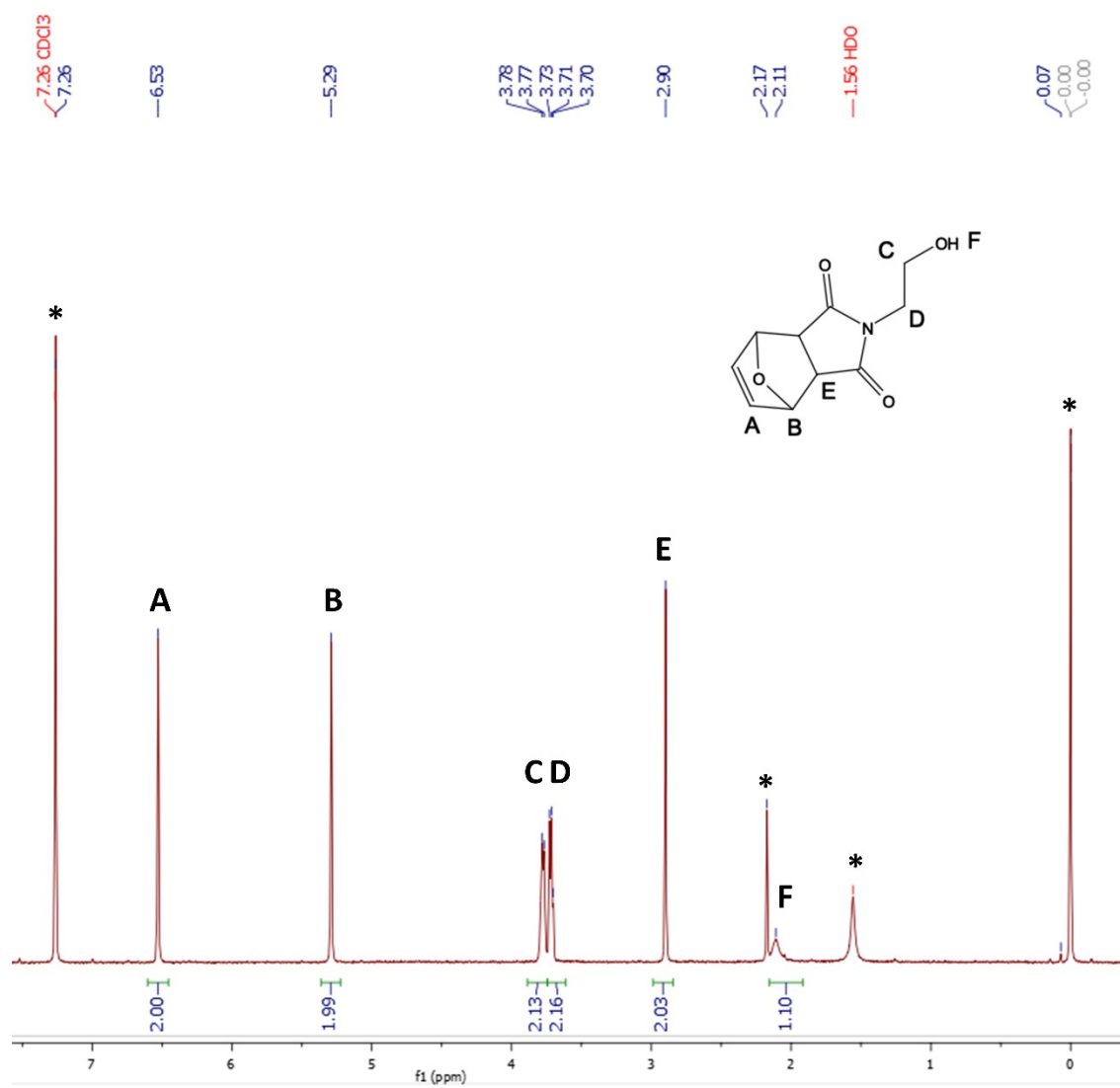


Figure S1: ¹H-NMR spectrum of compound **2** in CDCl₃ at 400 MHz. Peaks labelled * correspond to chloroform, acetone, water, and TMS from left to right.

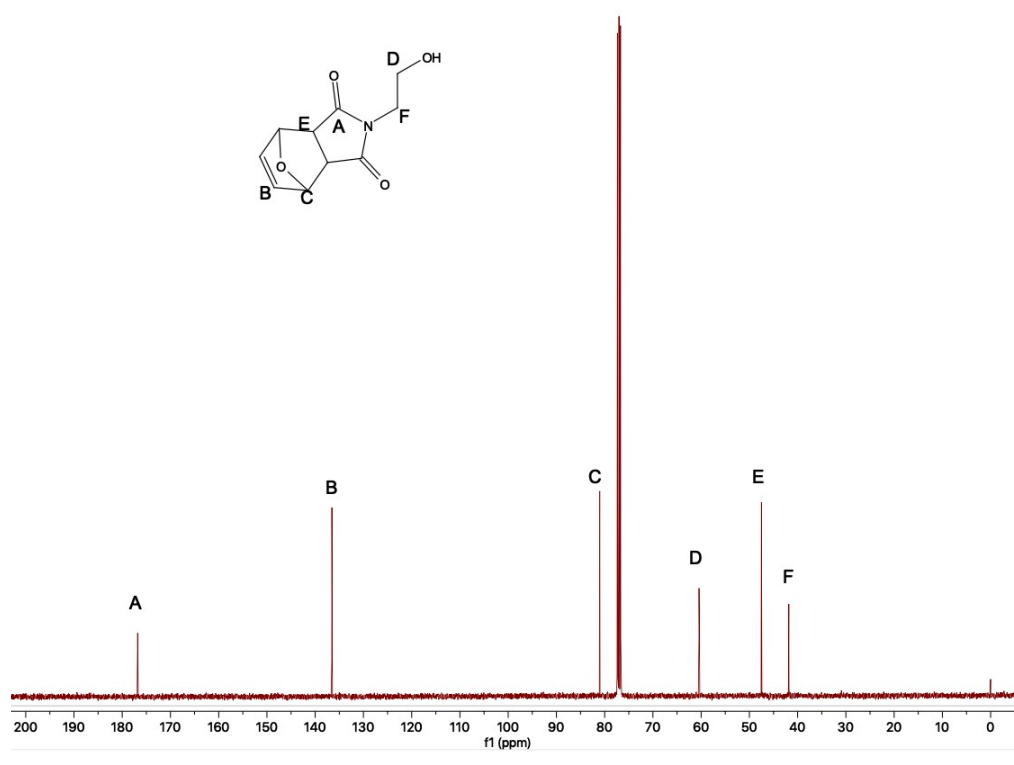


Figure S2: ^{13}C -NMR spectrum of compound **2** in CDCl_3 at 400 MHz.

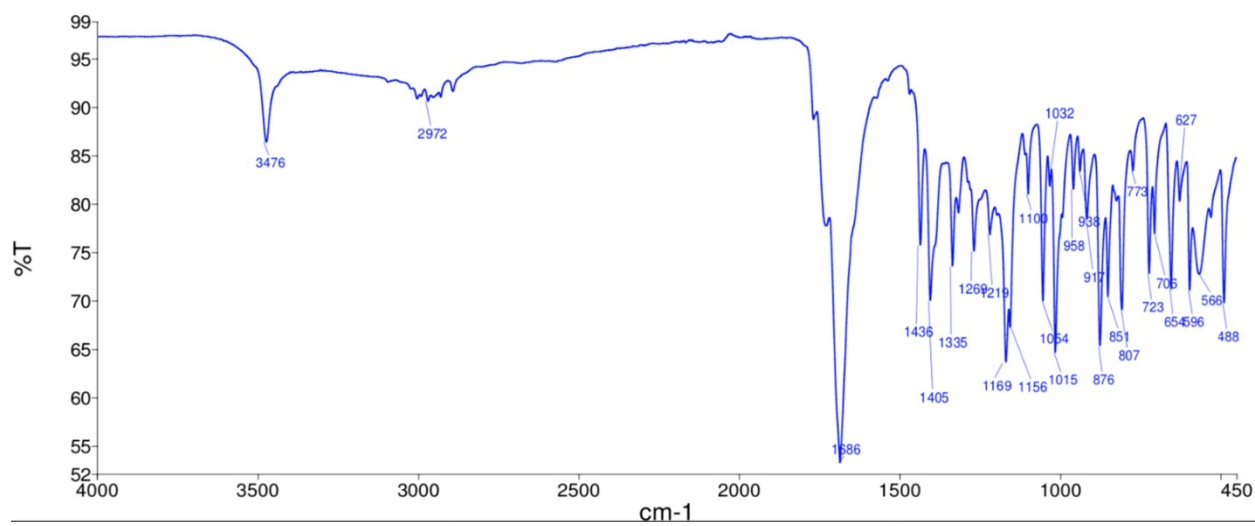


Figure S3: ATR-FTIR spectrum of compound **2**.

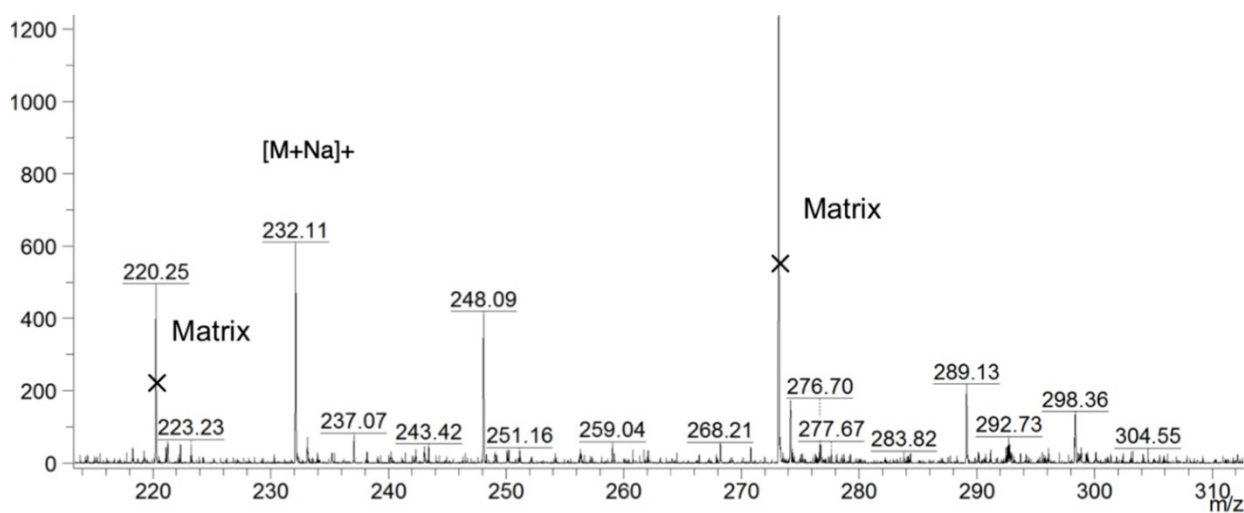


Figure S4: MALDI-TOF-MS spectrum of compound **2** on DCTB matrix.

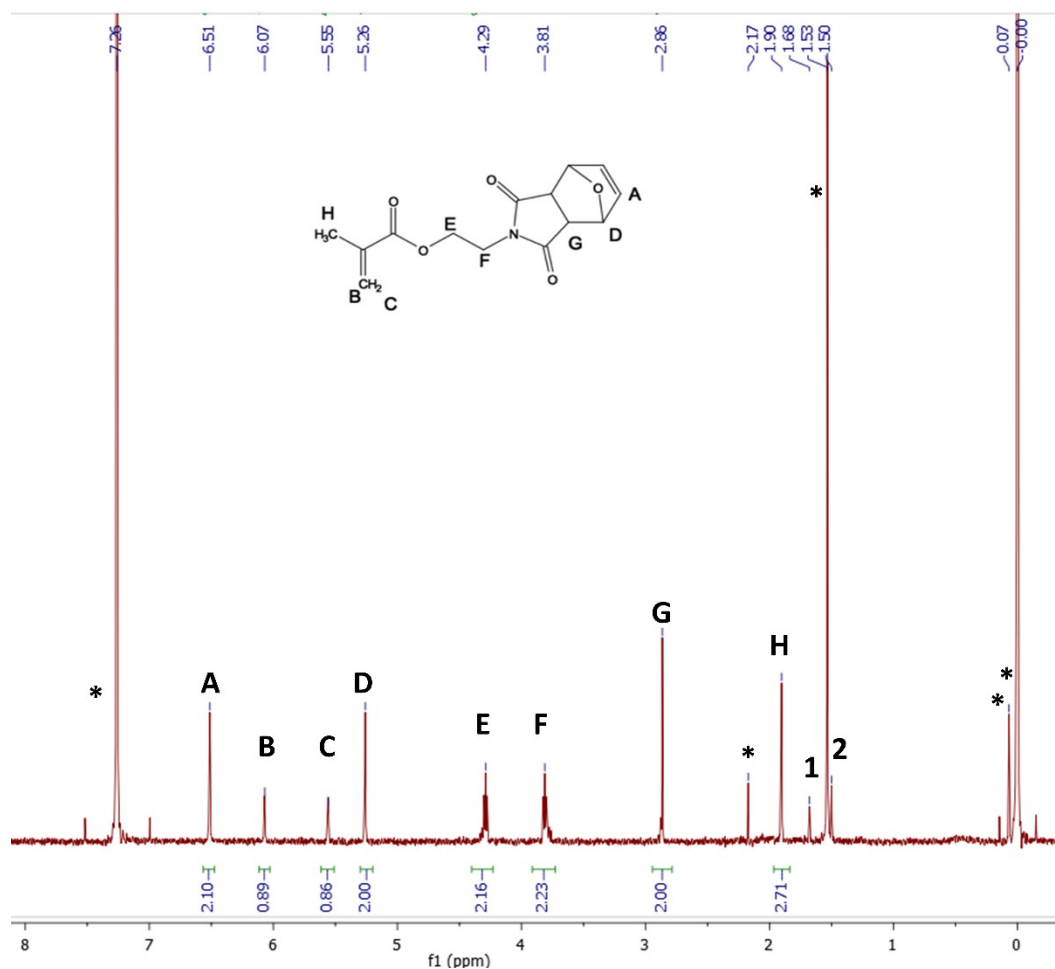


Figure S5: $^1\text{H-NMR}$ of compound **3** in CDCl_3 at 400 MHz. Peaks labelled * correspond to chloroform, acetone, water, silicon grease, and TMS from left to right. Two impurity peaks labelled 1 and 2 are observed, which likely arise from 6-chloro-3,4-dihydro-2,5-dimethyl-2H-pyran-2-carbonyl chloride, present in commercial methacryloyl chloride.³ This byproduct does not contain an acrylate moiety and therefore does not interfere in the polymerization.

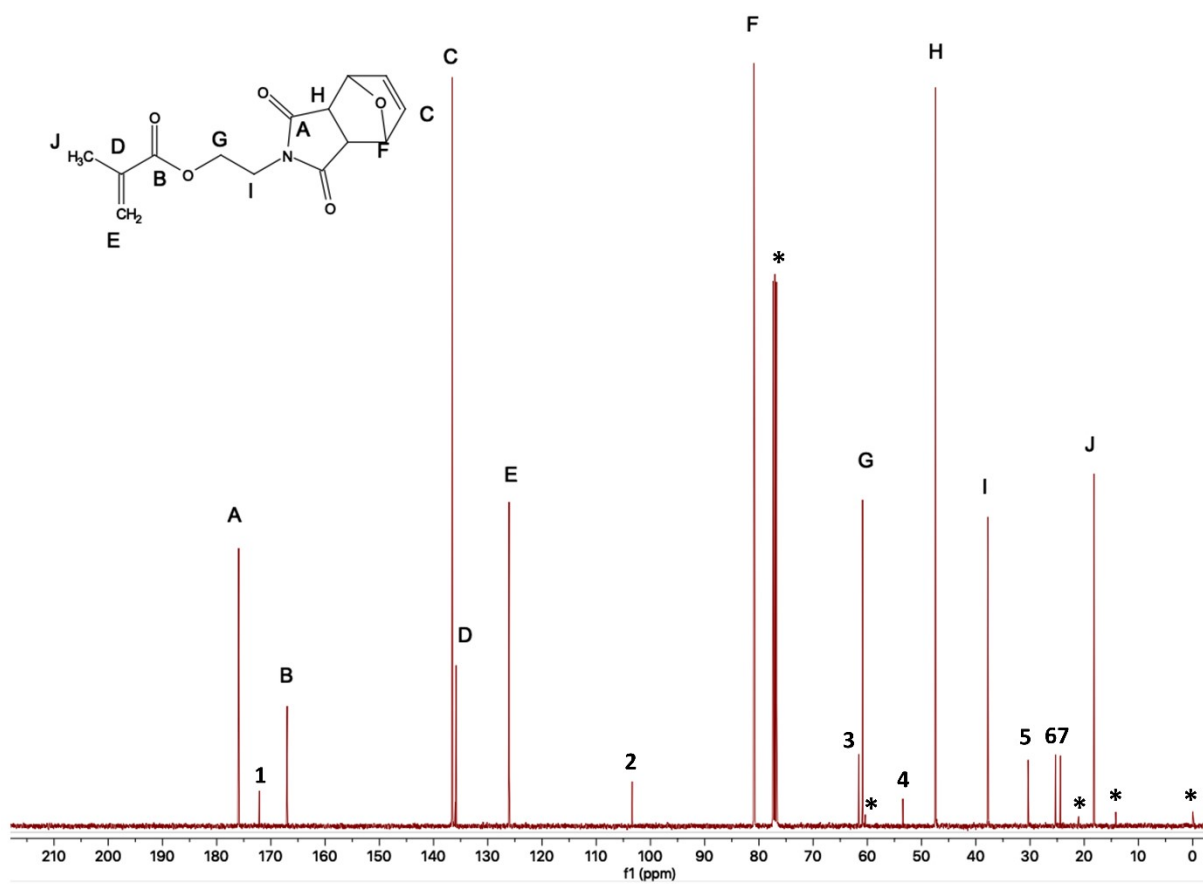


Figure S6: ¹³C-NMR of compound **3** in CDCl₃ at 400 MHz. Peaks indicated with * correspond to chloroform, ethyl acetate, and TMS. As indicated by Figure S5, the numbered peaks likely correspond to 6-chloro-3,4-dihydro-2,5-dimethyl-2H-pyran-2-carbonyl chloride.

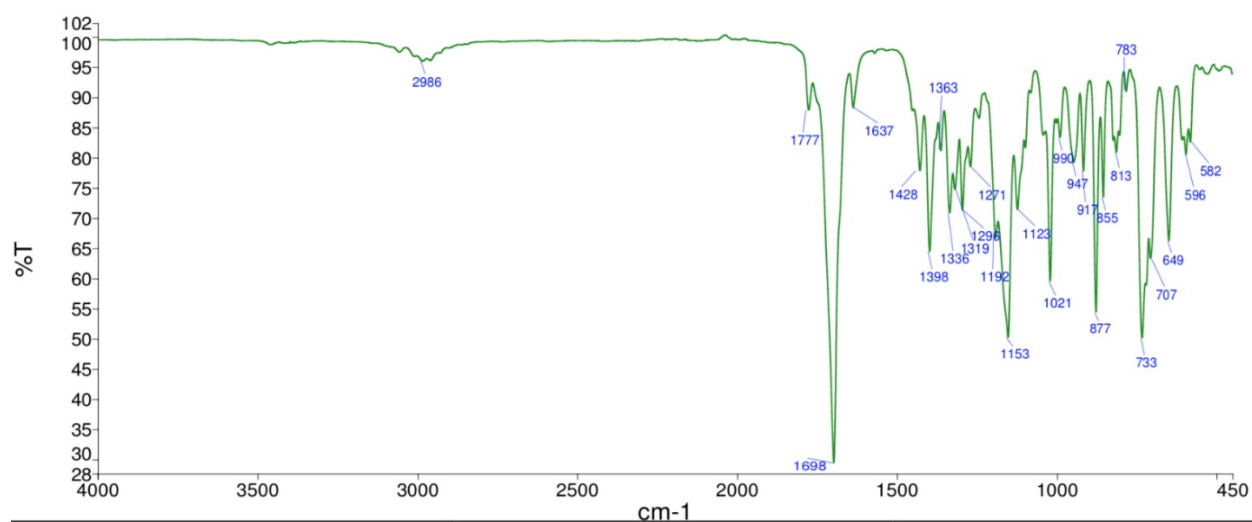


Figure S7: ATR-FTIR spectrum of compound **3**.

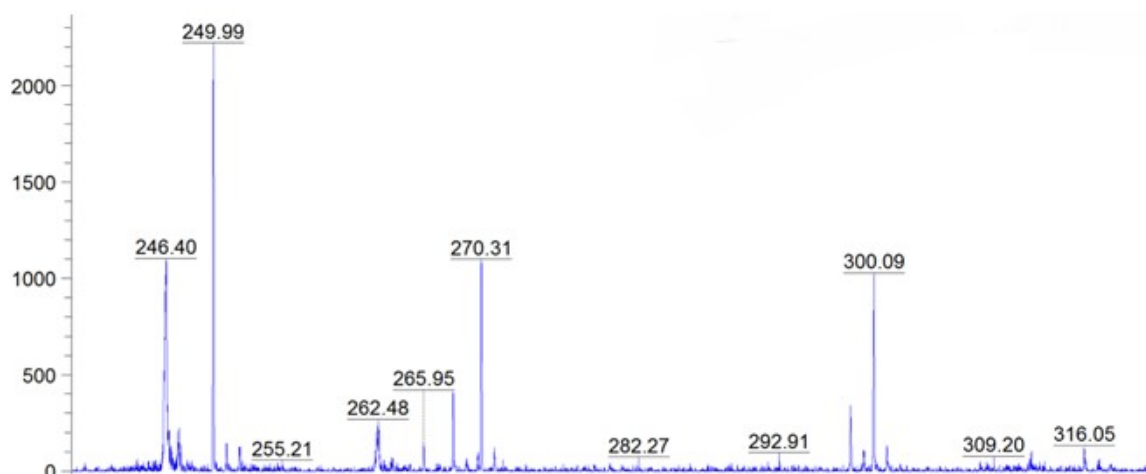
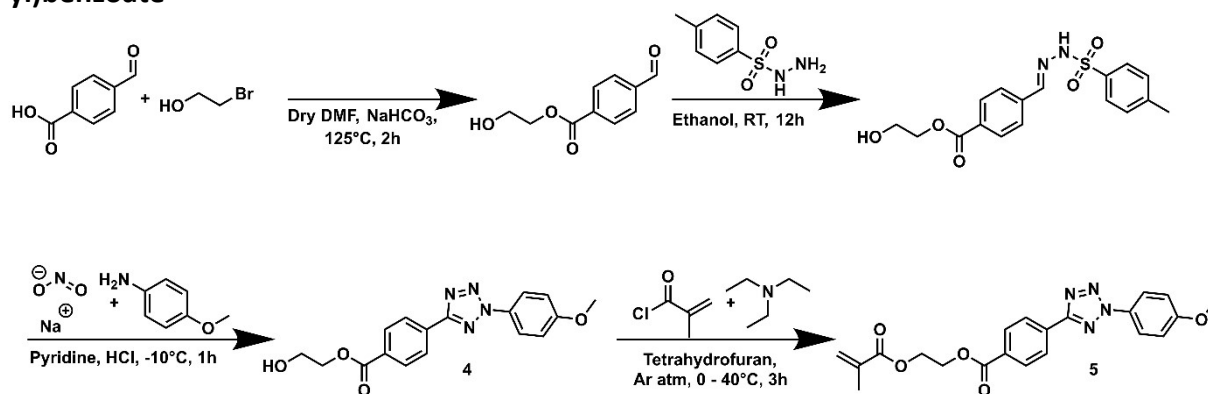


Figure S8: MALDI-TOF-MS spectrum of compound **3** on CHCA matrix.

2.1.2. Synthesis of 2-(methacryloyloxy)ethyl 4-(2-(4-methoxyphenyl)-2H-tetrazol-5-yl)benzoate



Intermediate **4** was synthesized following the literature procedure of Heiler *et al.*⁴

To obtain compound **5**, 961 mg of **4** (2.82 mmol, 1.00 eq.) was dissolved in 10 mL dry THF under argon atmosphere in a 100 mL round-bottom flask. 0.39 mL dry TEA (2.82 mmol, 1.00 eq.) in 10 mL dry THF was added. The mixture was cooled to 0 °C in an ice bath. 0.33 mL freshly distilled methacryloyl chloride (**17**) (3.39 mmol, 1.20 eq.) was added dropwise using a dropping funnel. After addition, the mixture was stirred for 12 h at 40 °C. The reaction mixture was added to 20 mL water and extracted using 30 mL dichloromethane. The organic layer was washed three times with 10 mL water, then dried over anhydrous magnesium sulphate. The solvent was removed under reduced pressure. The product was purified by flash column chromatography (SiO₂, 70:30 heptane : ethyl acetate) to yield **5** as an off-white powder (690 mg, 60%). To remove unreacted monomer, the solid was purified three times by trituration using diethyl ether, where the solvent was removed using decantation.

4: ¹H-NMR (400 MHz, CDCl₃): δ 8.34 (d, *J* = 8.0 Hz, 2H), 8.22 (d, *J* = 8.1 Hz, 2H), 8.12 (d, *J* = 8.7 Hz, 2H), 7.08 (d, *J* = 8.6 Hz, 2H), 4.52 (t, *J* = 4.7 Hz, 2H), 4.01 (q, *J* = 5.1 Hz, 2H), 3.91 (s, 3H), 1.97 (t, *J* = 6.0 Hz, 1H). ¹³C-NMR (399 MHz, CDCl₃): δ 166.38, 164.07, 160.73, 131.64, 131.43, 130.33, 126.95, 121.50, 114.77, 66.94, 61.42, 55.71. FTIR: $\tilde{\nu}$ = 3529, 2951, 1697, 1514, 1280, 1257, 1077, 1017, 866, 831, 737, 696, 506. MALDI-TOF-MS: Found [M+H]⁺ = 341.15 m/z. Calculated [M] = 340.12u, [M+H]⁺ = 341.12 u.

5: $^1\text{H-NMR}$ (400 MHz, CDCl_3): δ 8.38 – 8.29 (m, 2H), 8.24 – 8.16 (m, 2H), 8.16 – 8.06 (m, 2H), 7.14 – 7.02 (m, 2H), 6.15 (d, $J = 7.5$ Hz, 1H), 5.75 – 5.50 (m, 1H), 4.62 (dd, $J = 6.0, 3.5$ Hz, 2H), 4.53 (dd, $J = 5.9, 3.5$ Hz, 2H), 3.91 (s, 3H), 1.97 (t, $J = 1.3$ Hz, 3H). $^{13}\text{C-NMR}$ (399 MHz, CDCl_3): δ 167.18, 165.80, 164.10, 160.72, 135.95, 131.63, 131.40, 130.32, 126.96, 126.19, 121.49, 114.77, 62.93, 62.36, 55.71, 18.31. FTIR: $\tilde{\nu} = 3427, 3073, 3000, 2964, 2931, 2838, 2054, 2023, 1897, 1726, 1511, 1271, 1252, 1171, 1105, 1017, 833, 736, 620$. MALDI-TOF-MS: Found $[\text{M}+\text{Na}]^+ = 431.16$ m/z. Calculated $[\text{M}] = 408.14$ u, $[\text{M}+\text{Na}]^+ = 431.13$ u.

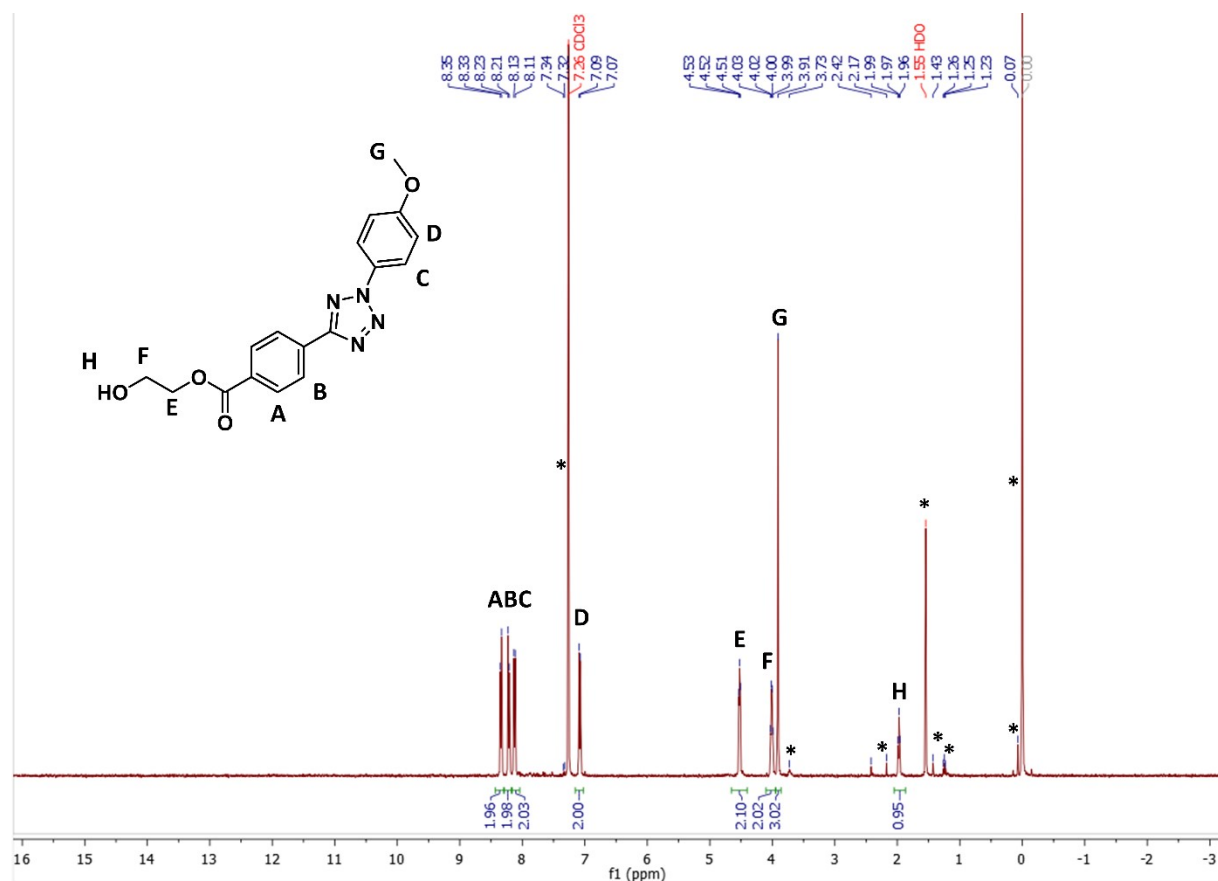


Figure S9: $^1\text{H-NMR}$ spectrum of compound **4** in CDCl_3 at 400 MHz. The peaks indicated with * correspond to chloroform, ethanol, acetone, water, silicon grease, and TMS.

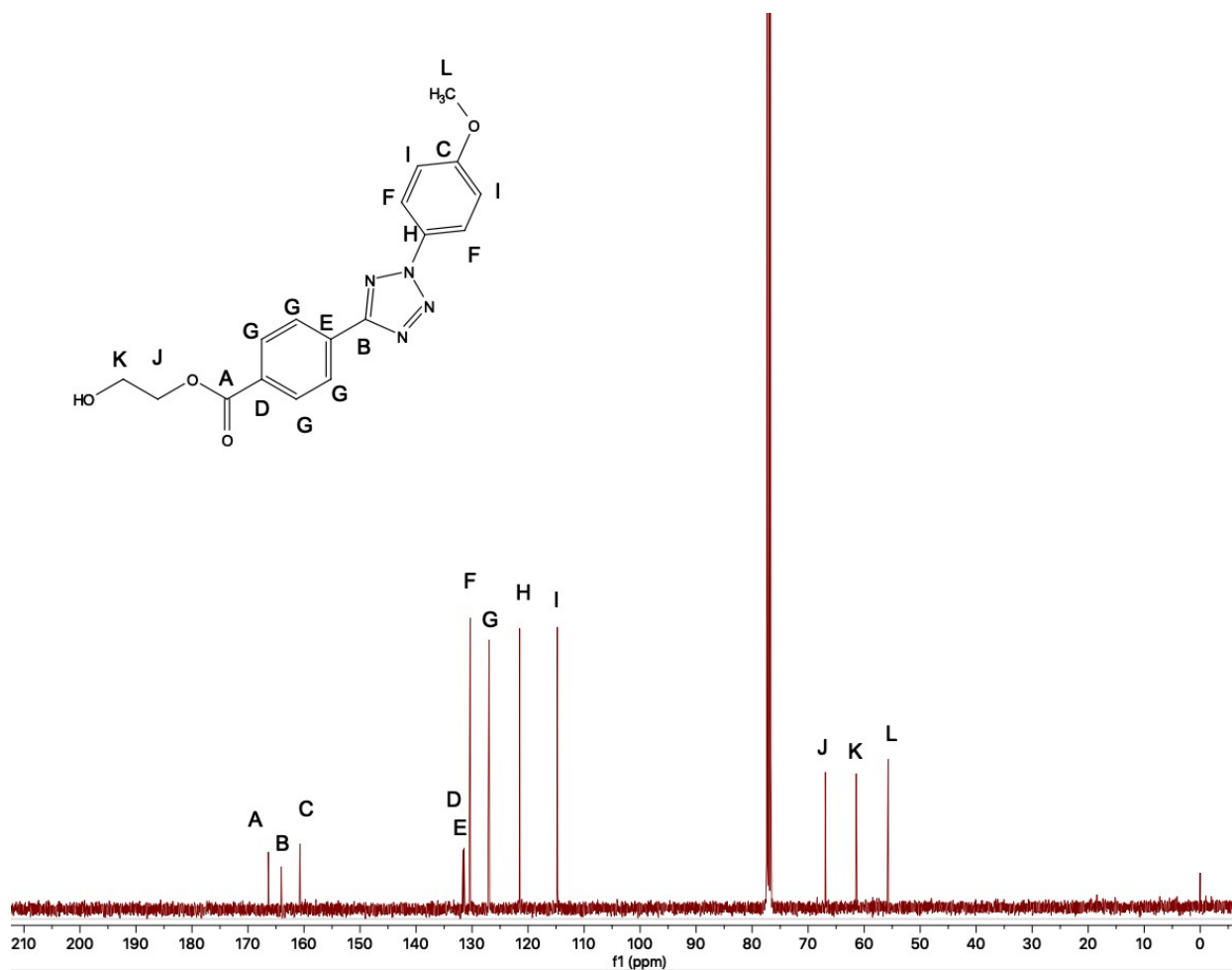


Figure S10: ^{13}C -NMR spectrum of compound 4 in CDCl_3 at 400 MHz.

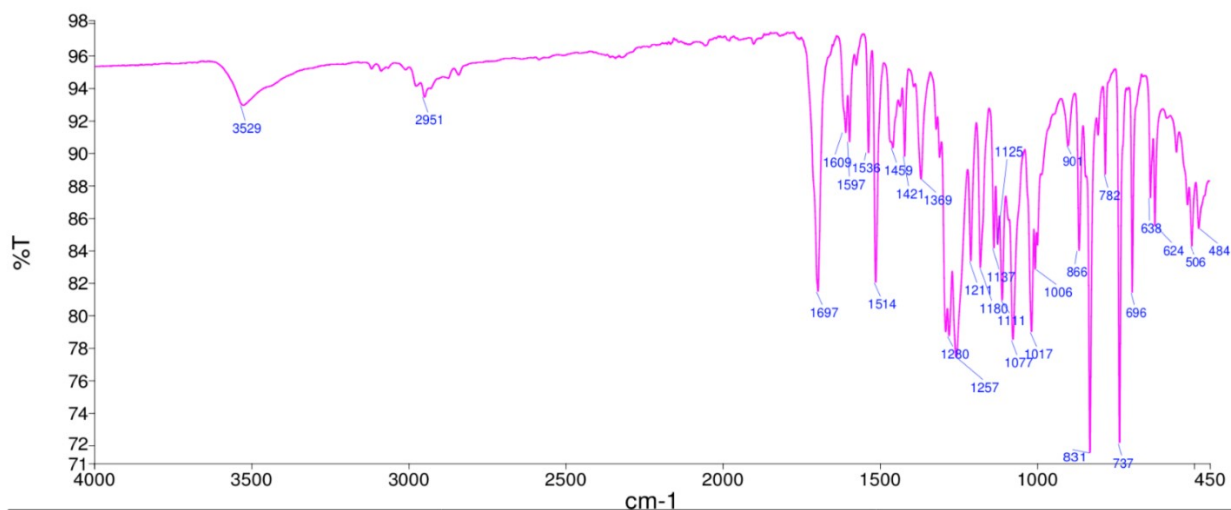


Figure S11: ATR-FTIR spectrum of compound 4.

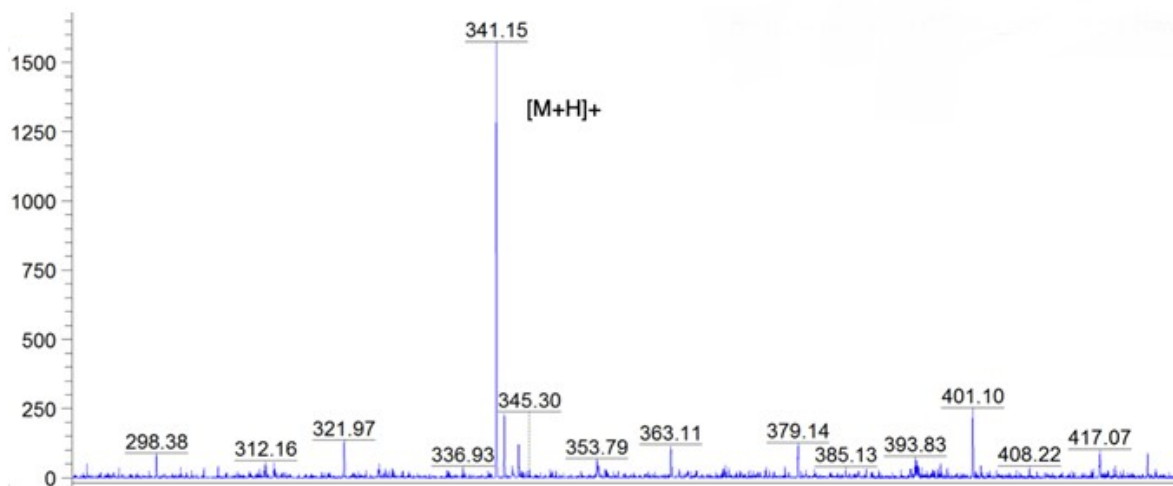


Figure S12: MALDI-TOF-MS spectrum of compound **4** on CHCA matrix.

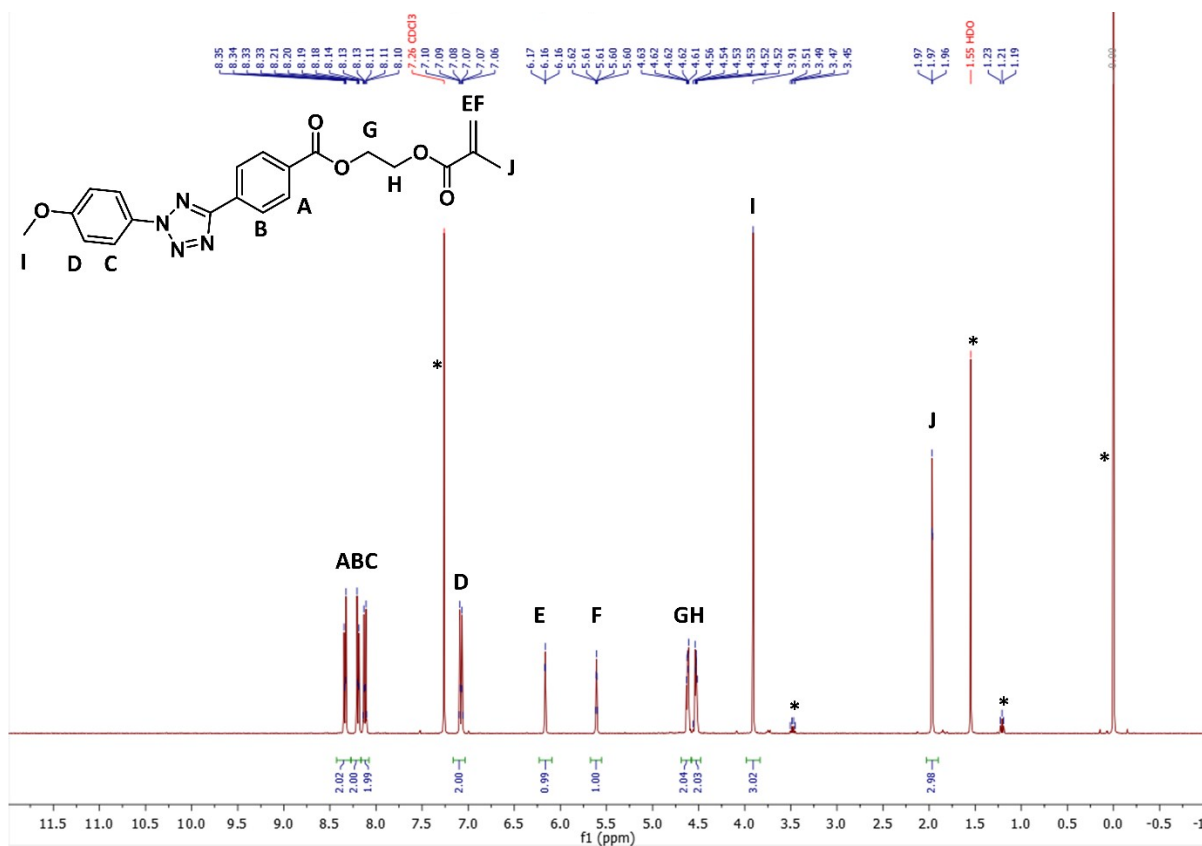


Figure S13: $^1\text{H-NMR}$ spectrum of compound **5** in CDCl_3 at 400 MHz. Peaks indicated with * correspond to chloroform, diethyl ether, water, and TMS.

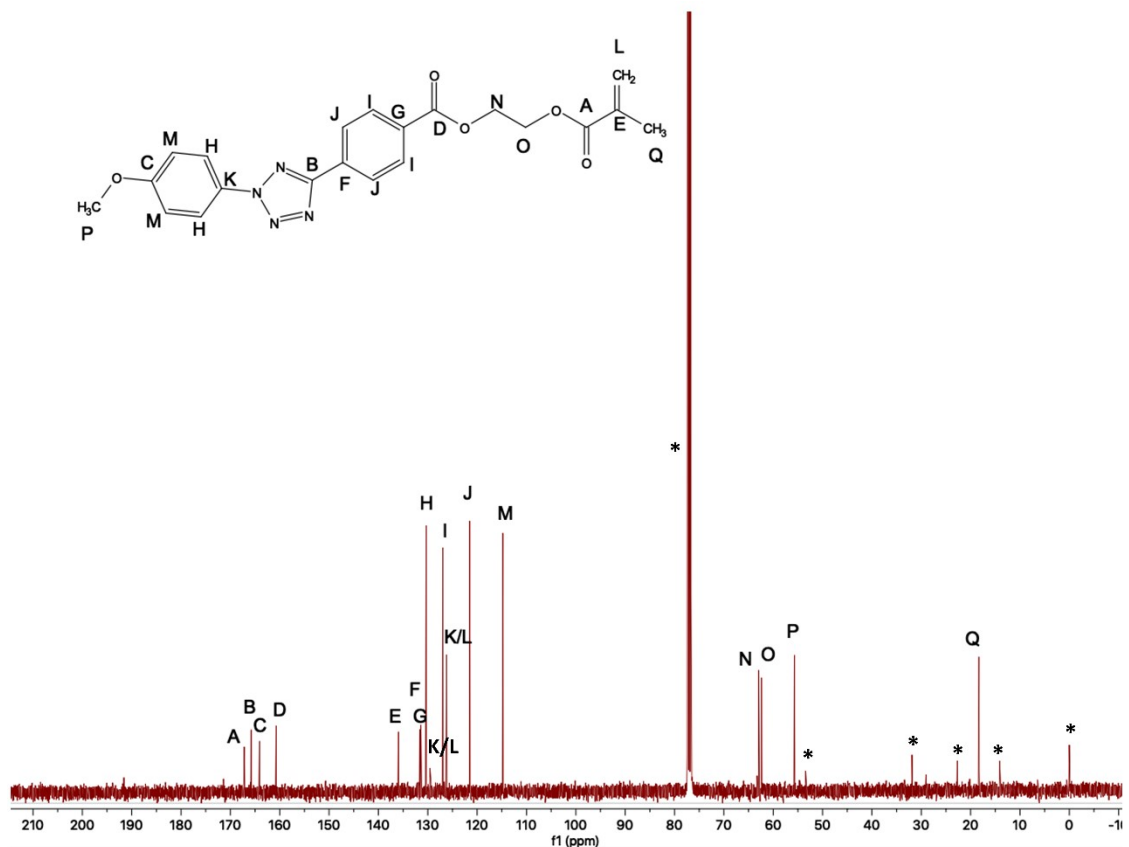


Figure S14: ^{13}C -NMR spectrum of compound 5 in CDCl_3 at 400 MHz. Peaks indicated with * correspond to chloroform, dichloromethane, heptane, and TMS.

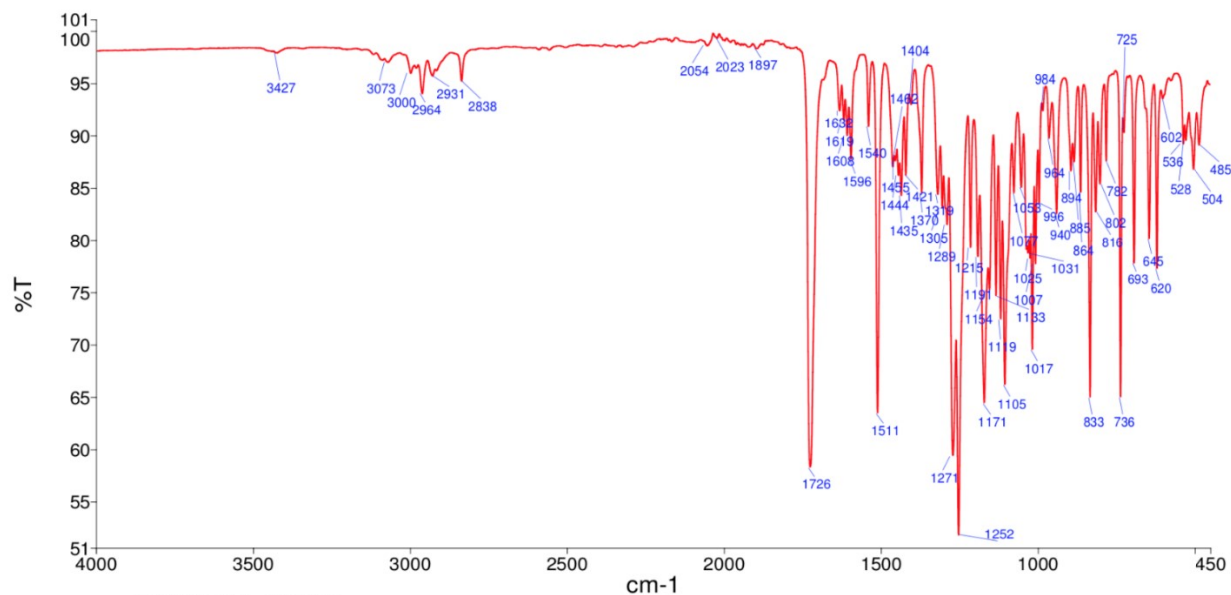


Figure S15: ATR-FTIR spectrum of compound 5.

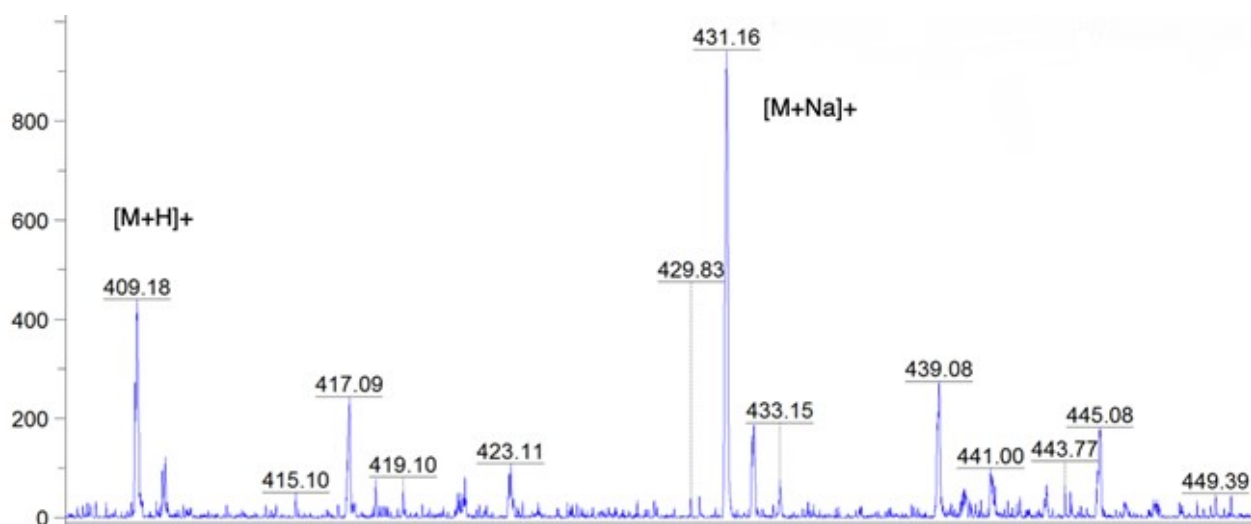


Figure S16: MALDI-TOF-MS spectrum of compound **5** on CHCA matrix.

2.2. Synthesis of random heterograft copolymers

2.2.1. Synthesis procedure

The synthesis of polymers **P1-P3** followed the same procedure, described here in detail for **P1**. Synthesis of **P2** and **P3** proceeded using 4-cyano-4-(phenylcarbonothioylthio)pentanoic acid N-succinimidyl ester instead of 4-cyano-4-(phenylcarbonothioylthio)pentanoic acid. Conversion was determined via $^1\text{H-NMR}$ after quenching. Incorporation ratio of grafts was determined via $^1\text{H-NMR}$ after workup. The degree of polymerization DP was then calculated as $\text{DP} = [\text{monomer}]_0 / [\text{RAFT}]_0 \cdot \text{conversion}$, with $[\text{monomer}]_0$ the total monomer feed concentration, and $[\text{RAFT}]_0$ the concentration of RAFT-agent.

Hereto, 76.20 mg of Tet (**5**) (187 μmol , 500 eq.), 57.30 mg of pMal (**3**) (207 μmol , 554 eq.), 107.50 mg dodecyl methacrylate (DodMA) (423 μmol , 1132 eq.), 1.58 g PEG methacrylate (oEGMA) (3.18 mmol, 8527 eq.), 5.86 mg 4-cyano-4-(phenylcarbonothioylthio)pentanoic acid (20.97 μmol , 56.2 eq.) and 526 μg AIBN (3.20 μmol , 8.58 eq.) were dissolved in 5 mL dry 1,4-dioxane in a Schlenk tube. PEG methacrylate and dodecyl methacrylate were passed over a short alumina column (DCM) to remove stabilizers. The mixture was degassed for 1 h using argon. After this, the mixture was placed in a 60 °C preheated oil bath for 14 h. The reaction was monitored by $^1\text{H-NMR}$ until a conversion of around 70% was observed. The reaction was quenched by immersing in liquid nitrogen. The mixture was precipitated in 1 L ice cold diethyl ether in which polymer **P1** precipitated as a viscous pink solid on the bottom (1.24 g, pale pink viscous solid).

P1: $^1\text{H-NMR}$ (400 MHz, CDCl_3): δ 8.51 – 7.97 (m), 7.94 – 7.42 (m), 7.10 (d, $J = 8.8$ Hz), 6.57 (s), 4.62 – 3.51 (br), 3.38 (br), 2.98 (m), 2.28 – 1.53 (br), 1.50 – 1.16 (br), 1.16 – 0.62 (br). DP = 193 r.u. $M_n = 90$ kg mol $^{-1}$. SEC (DMF, 10 mM LiBr): $\bar{D} = 1.33$.

P2: $^1\text{H-NMR}$ (399 MHz, CDCl_3): δ 4.28 – 3.40 (m), 3.38 (br), 1.92 (br), 1.28 (br), 1.10 – 0.63 (m). DP = 153 r.u. $M_n = 63$ kg mol $^{-1}$. SEC (DMF, 10 mM LiBr): $\bar{D} = 1.33$.

P3: $^1\text{H-NMR}$ (399 MHz, CDCl_3): δ 6.57 (br), 5.28 (br), 4.34 – 3.72 (m), 3.72 – 3.43 (m), 3.38 (s), 3.04 – 2.80 (m), 1.94 (br), 1.44 – 1.14 (m), 1.14 – 0.44 (m). DP = 206 r.u. $M_n = 90 \text{ kg mol}^{-1}$. SEC (DMF, 10 mM LiBr): $\bar{D} = 1.33$.

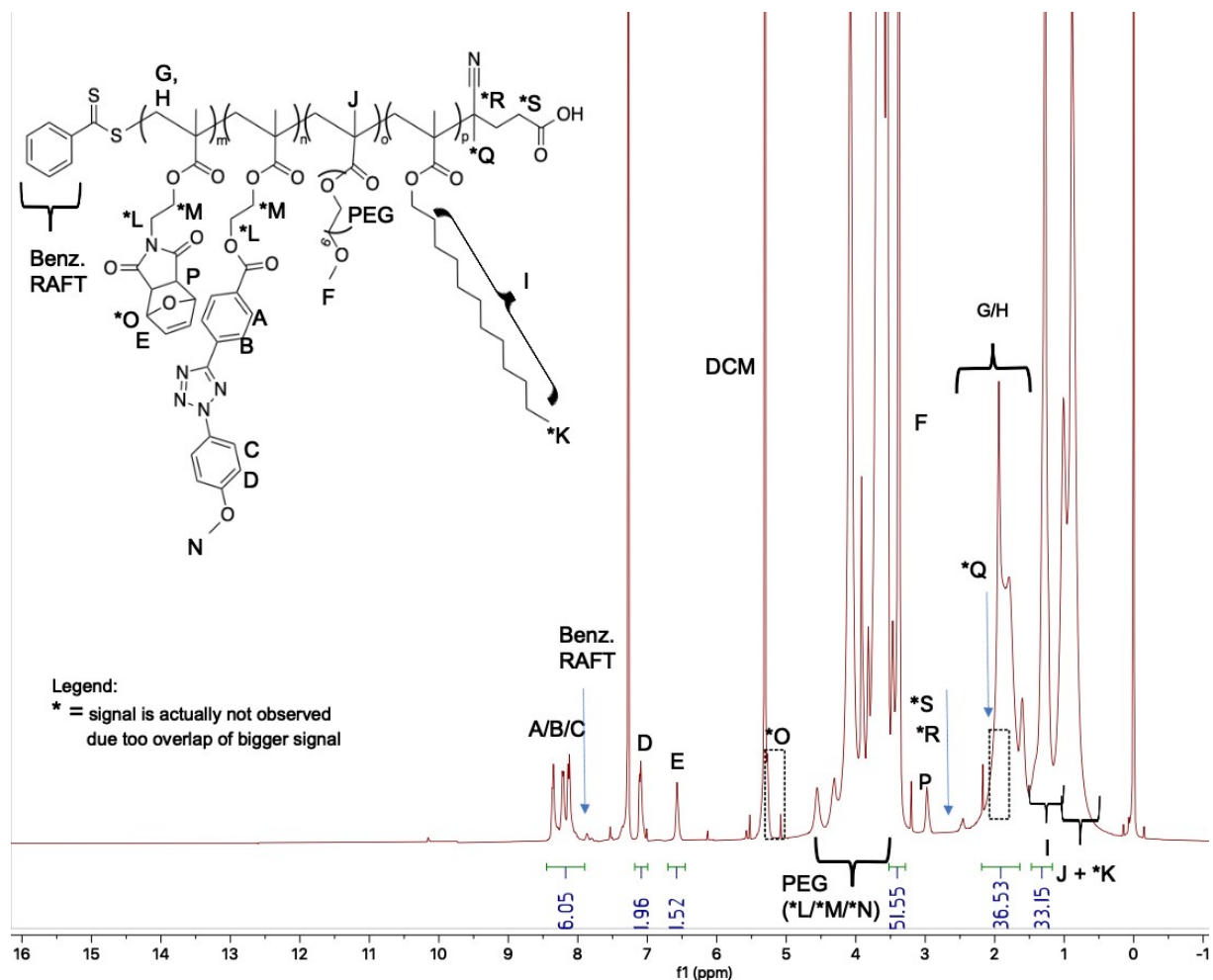


Figure S17: $^1\text{H-NMR}$ spectrum of **P1** in CDCl_3 at 400 MHz.

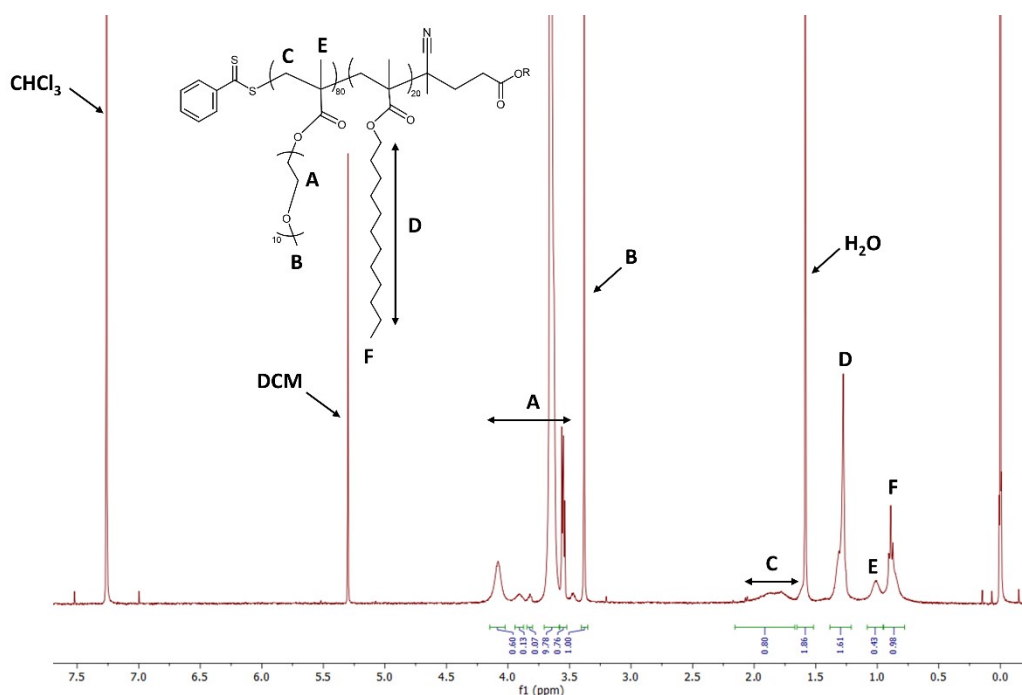


Figure S18: $^1\text{H-NMR}$ spectrum of **P2** in CDCl_3 at 400 MHz.

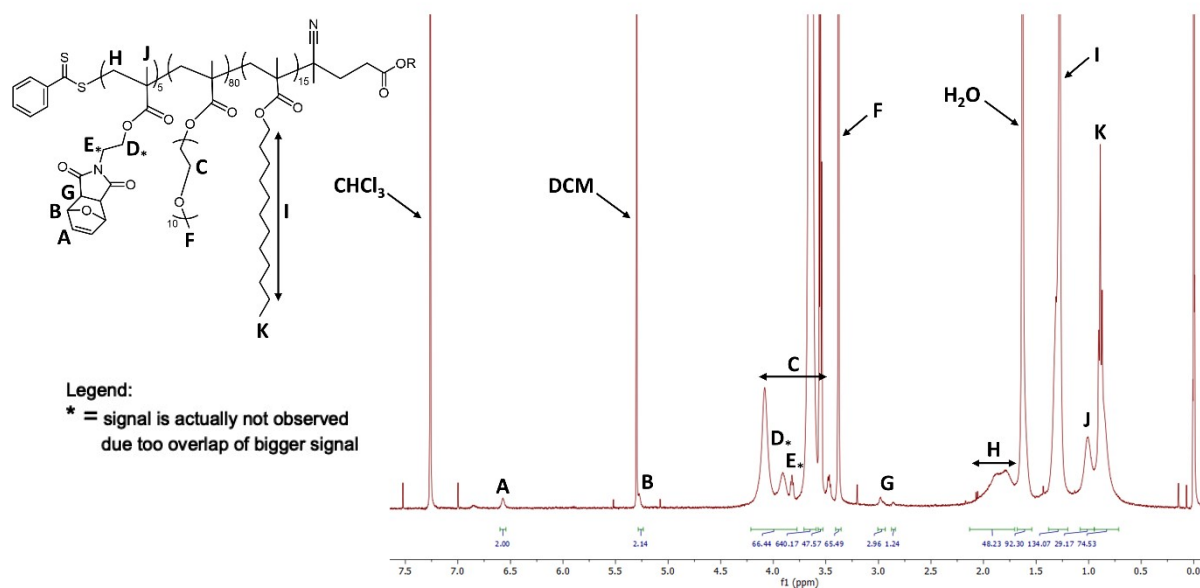
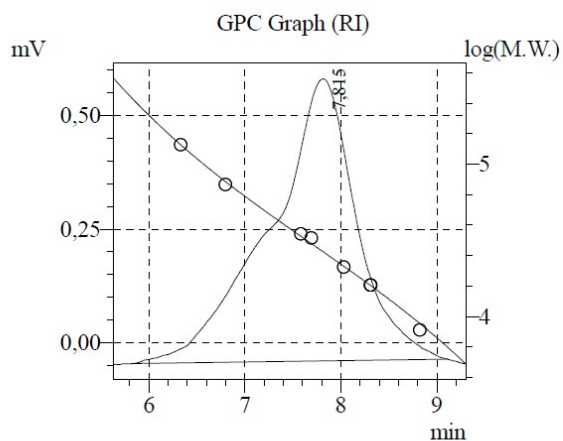


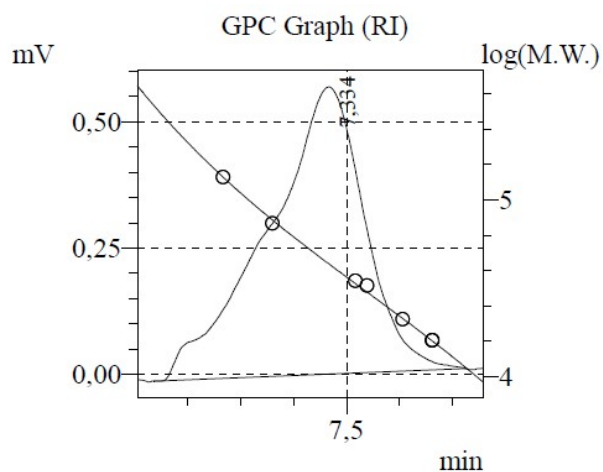
Figure S19: $^1\text{H-NMR}$ spectrum of **P3** in CDCl_3 at 400 MHz.



Total Average(RI)
Chromatogram Detector 2 Ch1

#	Mn	Mw	Mw/Mn
1	27931	37263	1.33411
	27931	37263	1.33411

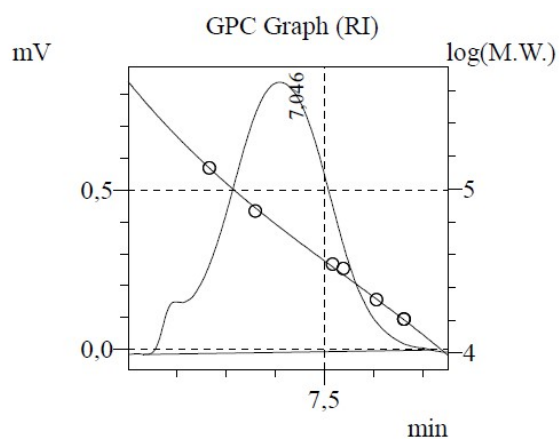
Figure S20: SEC trace of **P1** in DMF ($c_{P1} = 1 \text{ mg mL}^{-1}$).



Total Average(RI)
Chromatogram Detector 2 Ch1

#	Mn	Mw	Mw/Mn
1	48011	63779	1,32843
	48011	63779	1,32843

Figure S21: SEC trace of **P2** in DMF ($c_{P2} = 1 \text{ mg mL}^{-1}$).



Total Average(RI)

Chromatogram Detector 2 Ch1

#	Mn	Mw	Mw/Mn
1	54024	72090	1.33440
	54024	72090	1.33440

Figure S22: SEC trace of **P3** in DMF ($c_{P3} = 1 \text{ mg mL}^{-1}$).

2.2.2. Polymer conversion

Conversion was determined via $^1\text{H-NMR}$ by comparing the integrals of the unreacted methacrylate monomers (δ 5.5 – 6.5) with the backbone signal of the reacted monomers (δ 1.5 – 2.0). This is shown in Figure S20 for **P3**.

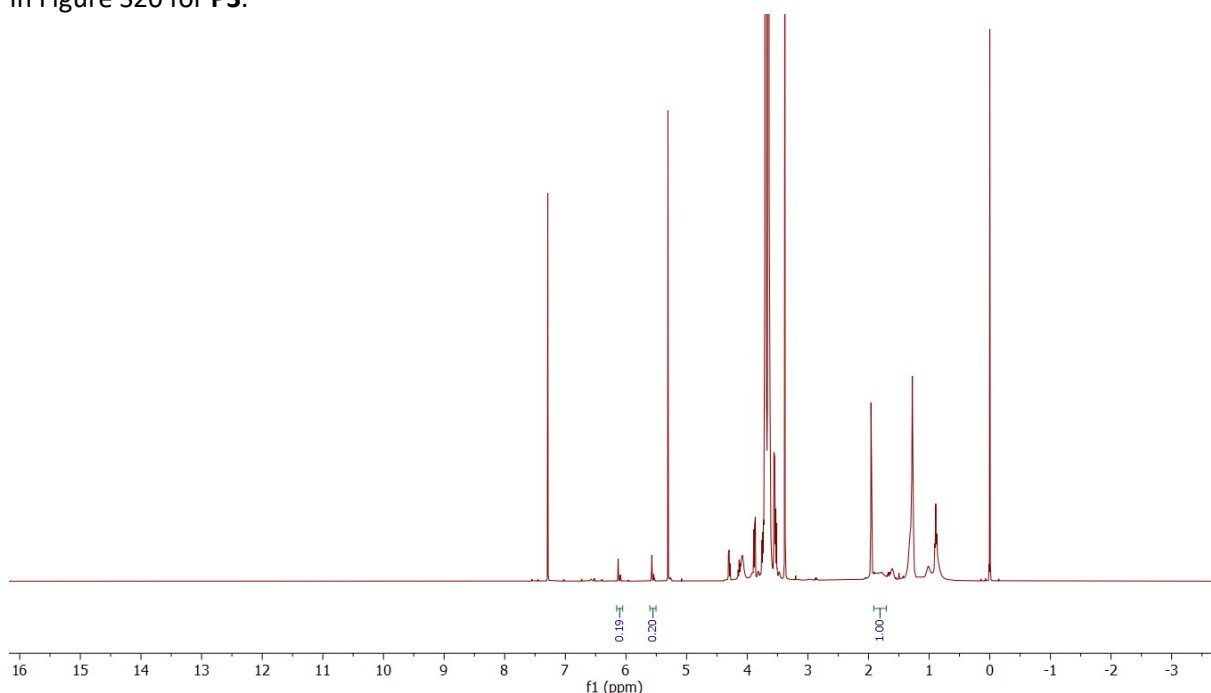


Figure S23: $^1\text{H-NMR}$ spectrum of **P3** in CDCl_3 at 400 MHz after quenching to determine the conversion.

Table S1: Monomer incorporation ratios of **P1-P3**, degree of polymerization DP, polymer molar mass M_n , and dispersity \bar{D} .

Polymer	oEGMA	DodMA	Tet	pMal	DP (-)	M_n (kg mol ⁻¹)	\bar{D} (SEC-DMF)
P1	0.83	0.09	0.05	0.04	193	90	1.33
P2	0.65	0.35	-	-	153	63	1.33
P3	0.74	0.22	-	0.04	206	90	1.33

2.3. Nanoparticle size

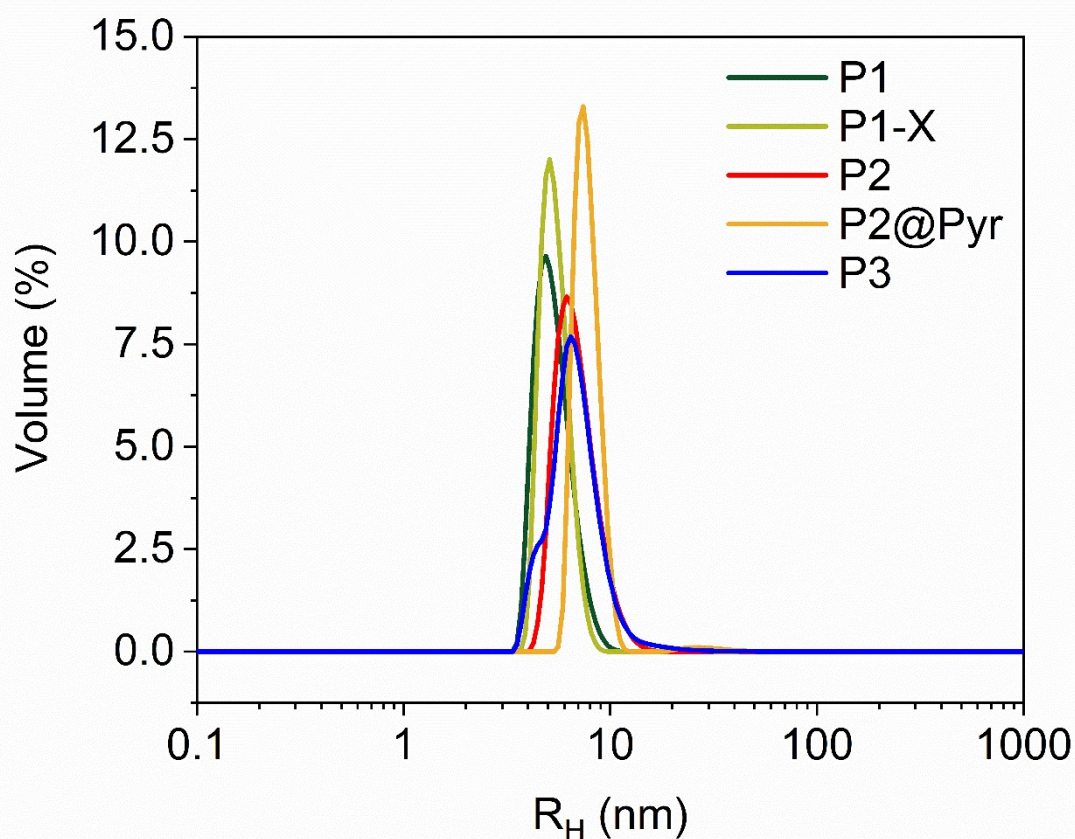
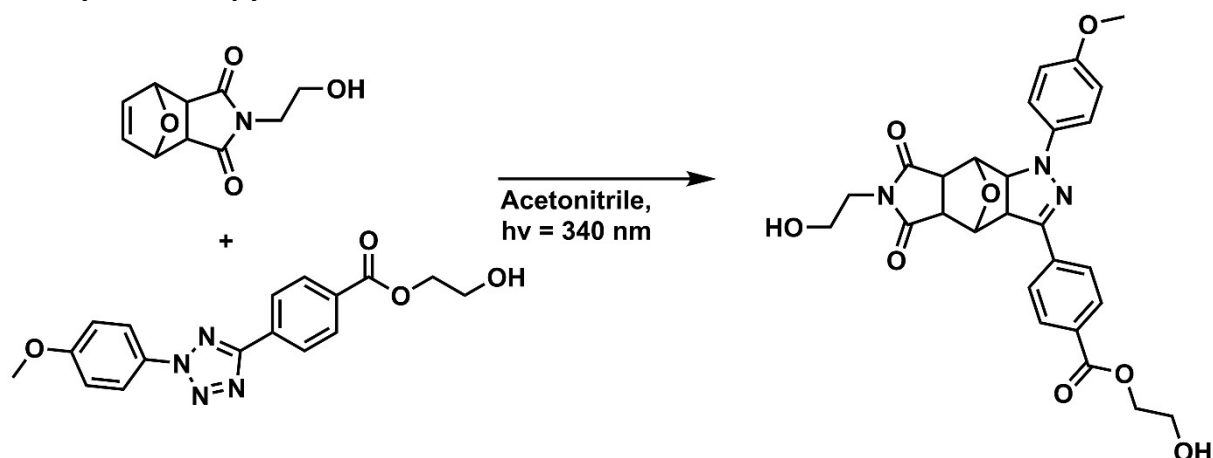


Figure S24: DLS volume plots of the hydrodynamic radius R_H measured at a 90° angle for polymer solutions of **P1-P3** in water at 1 mg mL⁻¹.

Table S2: Hydrodynamic radius of polymer solutions of **P1-P3** determined via DLS.

Polymer	R_H (nm)
P1	6.1 ± 1.3
P1-X	5.8 ± 0.9
P2	8.4 ± 2.3
P2@Pyr	7.8 ± 1.0
P3	8.4 ± 2.3

2.4. Synthesis of pyrazoline adduct



First, 10.18 mg Tet and 6.37 mg pMal were dissolved in 3.2 mL acetonitrile and transferred to a 10x10mm absorbance cuvette. The solution was illuminated with a 340 nm Thorlabs led at a current of 50 mA under continuous stirring and cooling for 12 h. The solvent was evaporated under reduced powder to give a dark yellow powder. The crude product was impregnated on celite and purified via flash column chromatography (SiO₂, 90:10 dichloromethane : methanol) to yield the pyrazoline adduct as a bright yellow powder (5.4 mg, 35%).

¹H-NMR (400 MHz, CDCl₃): δ 8.08 (d, J = 8.1 Hz, 2H), 7.76 (d, J = 8.1 Hz, 2H), 7.11 (d, J = 8.5 Hz, 2H), 6.92 (d, J = 8.5 Hz, 2H), 5.22 (s, 1H), 5.13 (s, 1H), 4.64 (d, J = 9.4 Hz, 1H), 4.50 (t, J = 4.6 Hz, 2H), 4.09 (d, J = 9.5 Hz, 1H), 4.00 (d, J = 5.3 Hz, 2H), 3.81 (s, 3H), 3.74 (dd, J = 14.4, 5.0 Hz, 4H), 3.32 – 3.11 (m, 2H), 1.54 (s, 7H).

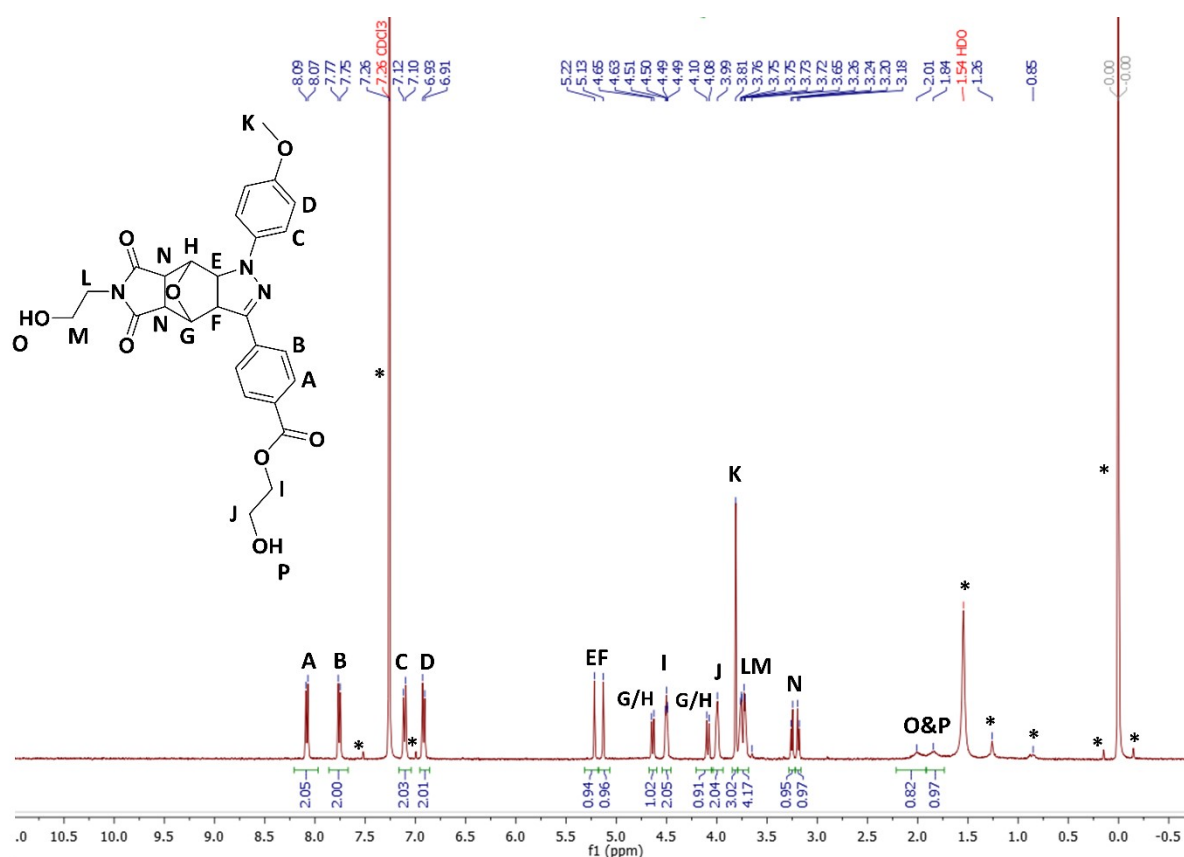


Figure S25: ¹H-NMR spectrum of the pyrazoline adduct **Pyr** in CDCl₃ at 400 MHz. The peaks indicated with * correspond to chloroform, water, heptane, and TMS.

2.5. Pyrazoline solvatochromism

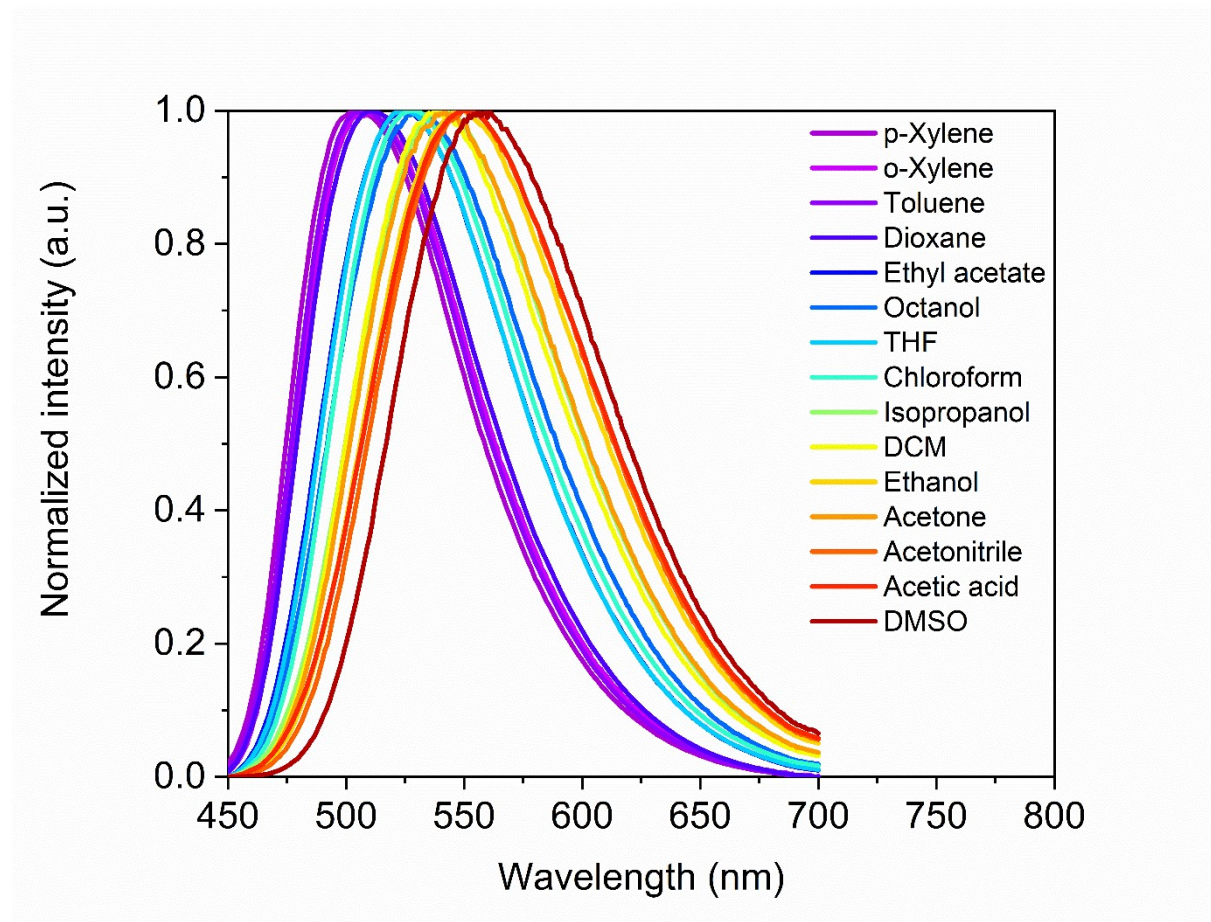


Figure S26: Normalized fluorescence spectrum of the pyrazoline adduct **Pyr** in solvents of increasing polarity. $\lambda_{\text{ex}} = 440 \text{ nm}$. $c_{\text{Pyr}} = 25 \mu\text{M}$.

The pyrazoline adduct was found to be insoluble in water, PBS, DMEM, and 10 vol% FBS in DMEM. Data is not shown, as no fluorescence was observed.

2.6. Pyrazoline UV-vis absorbance spectrum, extinction coefficient, and quantum yield

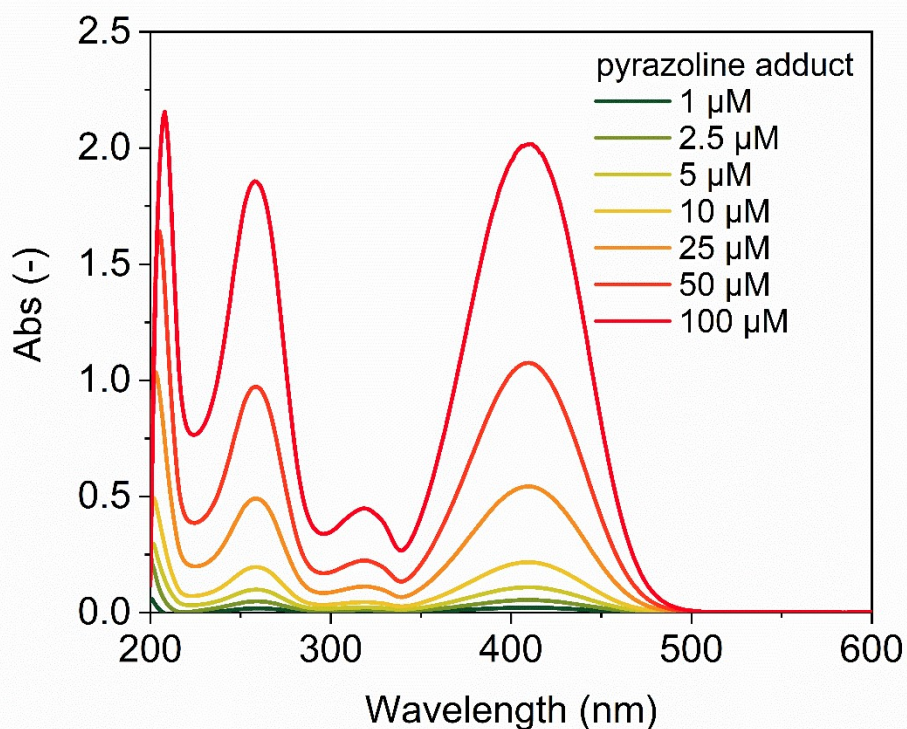


Figure S27: UV-vis absorbance spectrum of the pure pyrazoline adduct **Pyr** in isopropanol. $c_{\text{Pyr}} = 100 \mu\text{M}$.

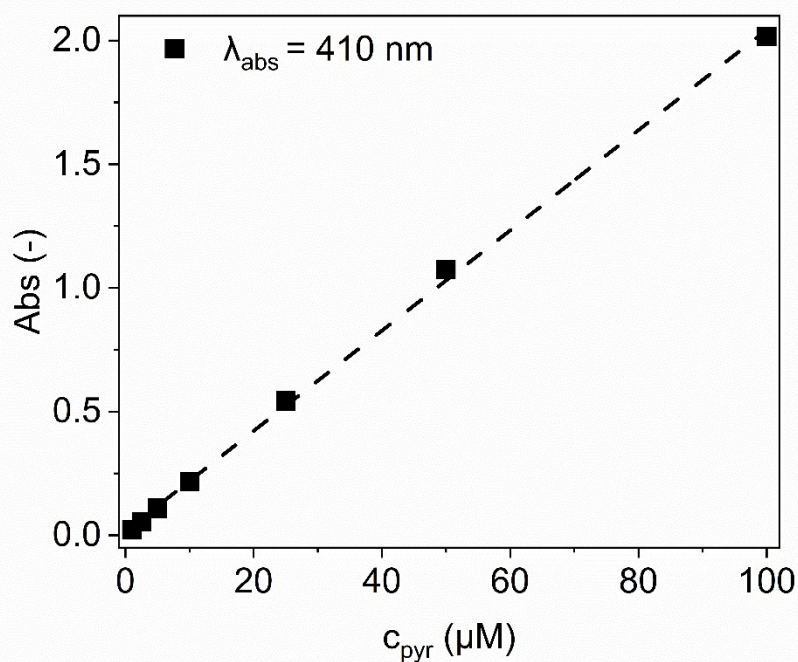


Figure S28: Plot of the UV-vis absorbance maxima of **Pyr** in isopropanol at $\lambda = 410 \text{ nm}$ for different concentrations. The molar absorption coefficient was calculated from the slope of a linear fit to the datapoints as $\epsilon = 20\,000 \text{ L mol}^{-1} \text{ cm}^{-1}$, goodness of fit $R^2 = 0.999$.

The fluorescence quantum yield of the pyrazoline adduct Pyr was determined using the comparative method against the dye coumarin 153 with a known fluorescence quantum yield of $\Phi_{\text{coum}} = 0.544$ (ethanol, $\lambda_{\text{ex}} = 402$ nm, $T = 298$ K).⁵ A concentration series of coumarin 153 and **Pyr** in ethanol was measured in triplicate with concentrations of 1, 2, 3, 4, and 5 μM , making sure the absorbance maximum stays below 0.1 to prevent fluorescence quenching effects. The absorbance spectra were recorded on an Agilent Cary 3500 UV-Vis with ethanol baseline correction using 10x10 mm cuvettes, shown in Figure S29. The fluorescence was measured on a Varian Eclipse Cary with ethanol baseline correction using 10x10 mm fluorescence cuvettes with an excitation wavelength of 402 nm, measured range $\lambda = 420 - 800$ nm, $V = 600$ Volt, 5 nm slit width, scan speed 120 nm/min, $T = 298$ K, shown in Figure S29. The absorbance at $\lambda = 402$ nm for the concentration series was plotted against the integrated fluorescence spectra in Figure S30 and the slope was calculated from a linear fit. The slopes were calculated as $\Delta_{\text{coum}} = 835585$, $R^2 = 1.000$; and $\Delta_{\text{pyr}} = 196544$, $R^2 = 0.999$. The fluorescence quantum yield of the pyrazoline adduct was subsequently determined using the following

$$\Phi_{\text{pyr}} = \Phi_{\text{coum}} \frac{\Delta_{\text{pyr}} n_{\text{pyr}}^2}{\Delta_{\text{coum}} n_{\text{coum}}^2}$$

formula: Φ is the fluorescence quantum yield of coumarin 153 ($\Phi_{\text{coum}} = 0.544$) and the pyrazoline adduct respectively, Δ is the observed slope in the absorbance vs integrated fluorescence plot, and n is the refractive index of the solvent, which

is equal for both solvents, hence $n_{\text{pyr}}^2/n_{\text{coum}}^2 = 1$. It follows that $\Phi_{\text{pyr}} = 0.544 \frac{196544}{835585} = 0.128$.

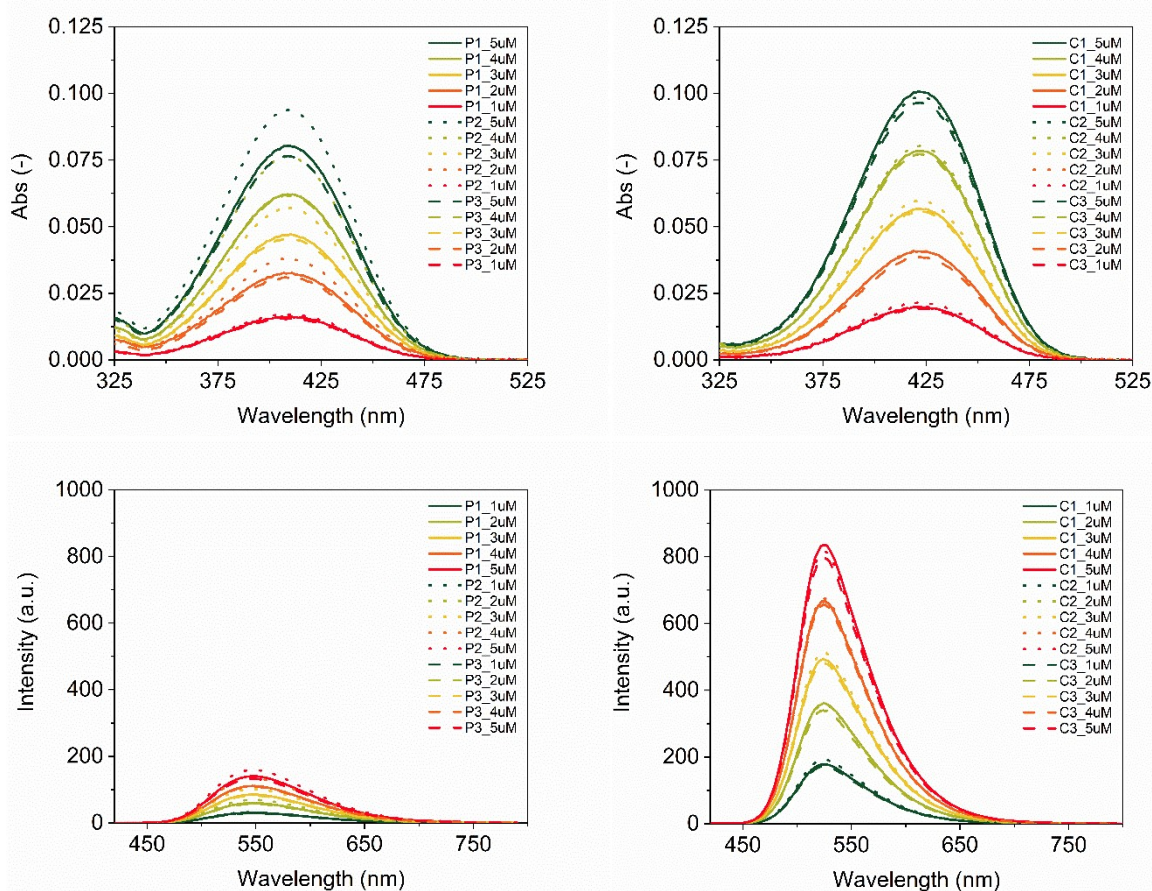


Figure S29: Plot of the UV-vis absorbance spectra of A) **Pyr** and B) coumarin 153 in ethanol for different concentrations. Fluorescence spectra of C) **Pyr** and D) coumarin 153 in ethanol for different concentrations. In the legend, C stands for coumarin 153, P stands for **Pyr**. The

experiment was measured in threefold (P1, P2, and P3; C1, C2, and C3 respectively). The concentration is given in μM .

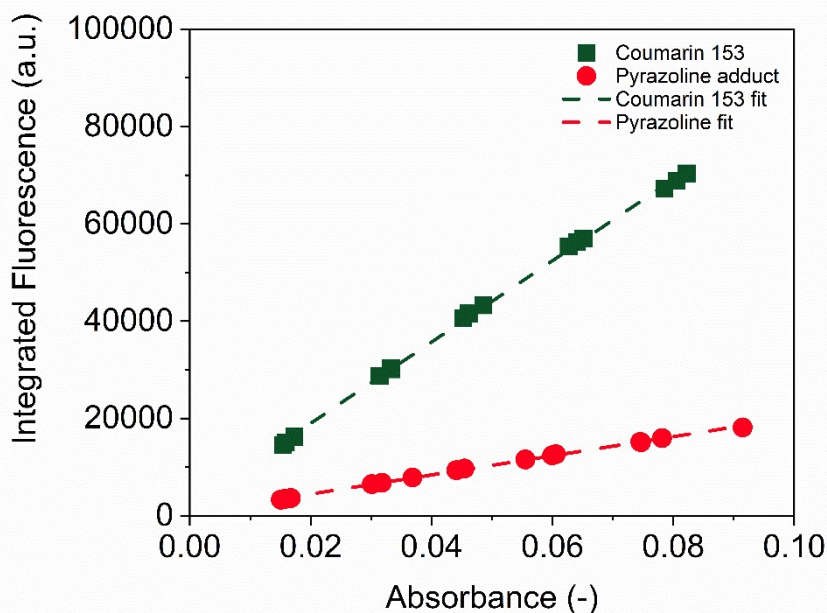


Figure S30: Plot of the UV-vis absorbance maxima at $\lambda = 402 \text{ nm}$ of **Pyr** and coumarin 153 against the corresponding integrated fluorescence spectra using $\lambda_{\text{ex}} = 402 \text{ nm}$. The linear fits have a slope of $\Delta_{\text{coum}} = 835585$, $R^2 = 1.000$ for coumarin 153; and $\Delta_{\text{pyr}} = 196544$, $R^2 = 0.999$ for **Pyr**.

2.7. Pyrazoline formation in **P1** and **P3**

Pyrazoline formation in **P1** and **P3** proceeded via UV-light irradiation of 1 mg mL^{-1} polymer solutions in water. The solution was illuminated with a 340 nm Thorlabs led at a current of 50 mA under continuous stirring and cooling for 105 min in the case of **P1** and 5 h in the case of **P3**. For **P3**, 1.2 eq. of tetrazole were added to the solution prior to illumination. Successful pyrazoline formation followed from the appearance of the pyrazoline UV-vis absorbance peak and characteristic fluorescence, given below in Figures S31-S32. The amount of the limiting reactant pMal, for **P1** and **P3** was calculated using the polymer properties given in Table S1. The final conversion was calculated from the pyrazoline UV-vis absorbance maximum around $\lambda = 410 \text{ nm}$, given in Table S3.

The fluorescence quantum yield of the polymers in water can be estimated from the absorbance at $\lambda = 440 \text{ nm}$ in Figure S31 and integrated fluorescence coming from the pyrazoline adduct at very low concentrations from Figure S32. At higher conversions, fluorescence quenching for **P1** and **P3** is clearly visible from Figure S32. Hence, we calculate the fluorescence quantum yield for **P3** after 5 minutes of cross-linking and obtain $\text{Abs}_{440} = 0.031$, an integrated fluorescence of 5578 a.u. . This yields us $\Delta\text{P3} = 166419$, and $\Phi_{\text{P3}} = 0.11$, similar to $\Phi_{\text{pyr}} = 0.128$ obtained in ESI section 2.6.

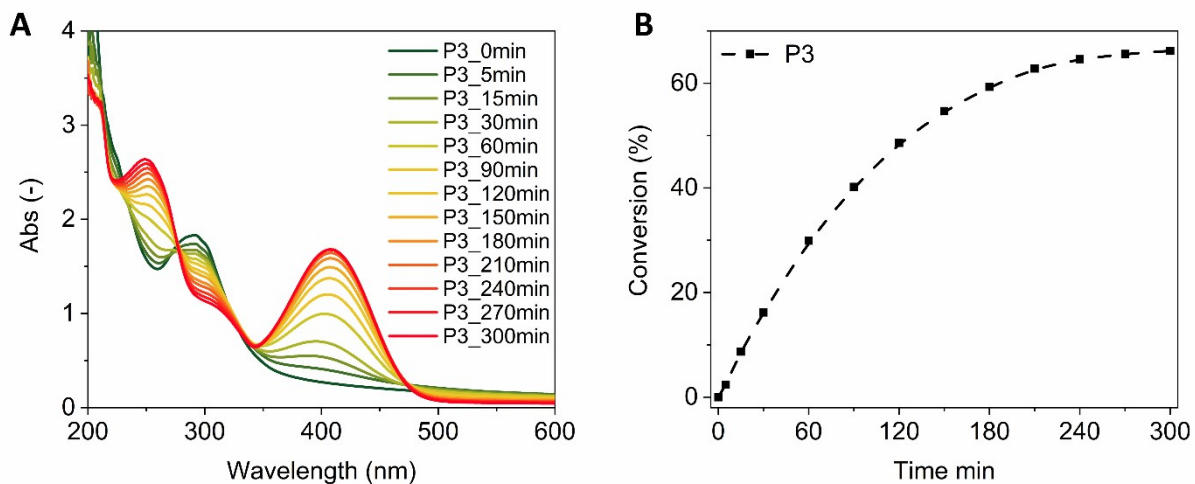


Figure S31: (A) Evolution of absorbance spectra during photoirradiation of **P3** in water. $c_{\text{pol}} = 1 \text{ mg mL}^{-1}$. (B) Conversion of pMal into pyrazoline adduct over time. The dashed line is added to guide the eye.

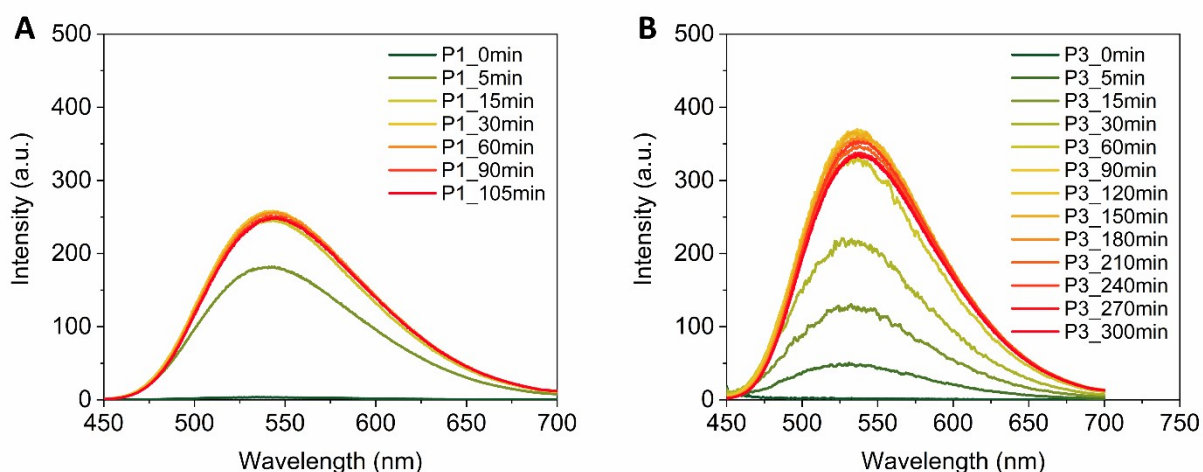


Figure S32: Evolution of fluorescence spectra during photoirradiation of (A) **P1** and (B) **P3** in water. $c_{\text{pol}} = 1 \text{ mg mL}^{-1}$. $\lambda_{\text{ex}} = 440 \text{ nm}$.

Table S3: Conversion of pMal into **Pyr** adduct for **P1-X** and **P3-G**. #pyrazoline corresponds to the number of pyrazoline adducts formed per polymer chain.

Sample	$c_{\text{pMal}} (\mu\text{M})$	Abs (-)	$c_{\text{Pyr}} (\mu\text{M})$	Conversion (%)	#pyrazoline
P1-X	0.080	0.90	0.045	56	4.3
P3-G	0.117	1.68	0.078	66	5.4

2.8. Pyrazoline adduct long-term stability

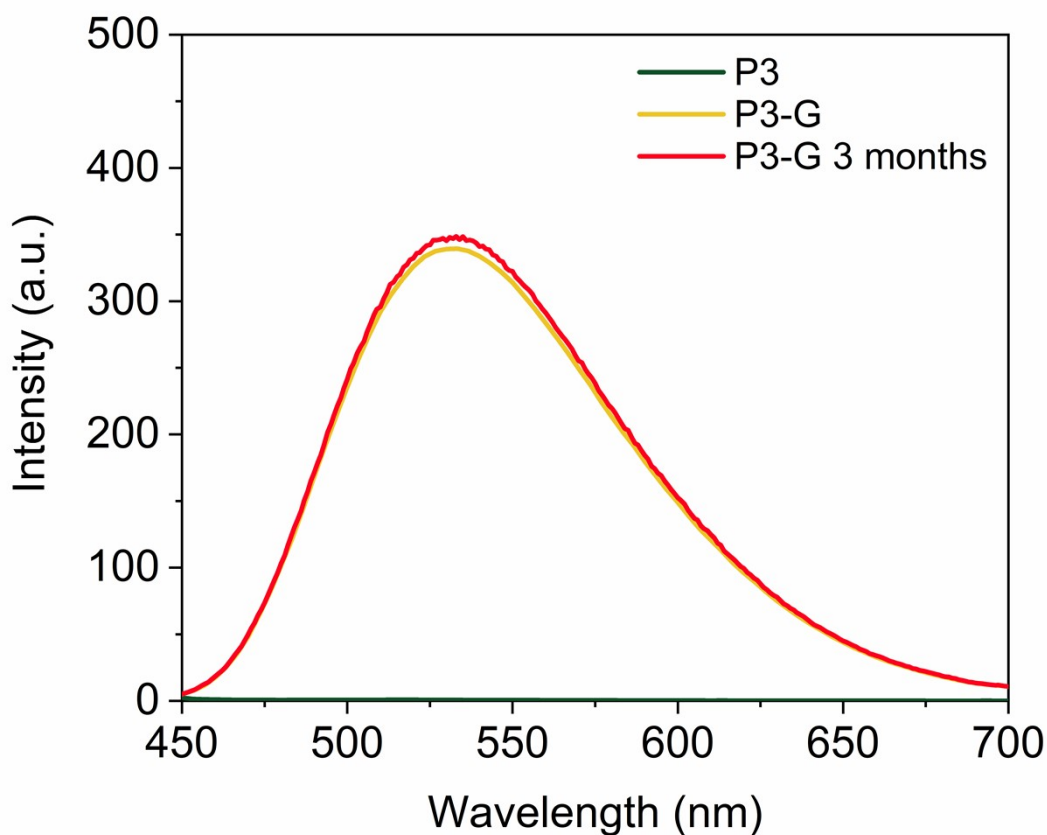


Figure S33: P3 fluorescence spectra before (**P3**) and after photoirradiation (**P3-G**) of **P3** in water, repeated after 3 months storage at ambient conditions. $c_{\text{pol}} = 1 \text{ mg mL}^{-1}$. $\lambda_{\text{ex}} = 440 \text{ nm}$.

3. References

- 1 C. Bolm, C. L. Dinter, A. Seger, H. Höcker and J. Brozio, *J. Org. Chem.*, 1999, **64**, 5730–5731.
- 2 G. Mantovani, F. Lecolley, L. Tao, D. M. Haddleton, J. Clerx, J. J. L. M. Cornelissen and K. Velonia, *J. Am. Chem. Soc.*, 2005, **127**, 2966–2973.
- 3 J. Warneke, Z. Wang, M. Zeller, D. Leibfritz, M. Plaumann and V. A. Azov, *Tetrahedron*, 2014, **70**, 6515–6521.
- 4 C. Heiler, J. T. Offenloch, E. Blasco and C. Barner-Kowollik, *ACS Macro Lett.*, 2017, **6**, 56–61.
- 5 K. Rurack and M. Spieles, *Anal. Chem.*, 2011, **83**, 1232–1242.